processes

MDPI

Article

Sedimentary Environment and Organic Matter Enrichment Model of Saline Lake Source Rock in the Linhe Depression, Hetao Basin, China

Xiaoyan Fu [1], Jungang Lu [1,*], Yulei Shi [2], Ranran Zhou [2], Shijia Chen [1] and Man Yuan [1]

[1] School of Geoscience and Technology, Southwest Petroleum University, Chengdu 610500, China; 202111000037@stu.swpu.edu.cn (X.F.); csj199131010015@163.com (S.C.); 202221000046@stu.swpu.edu.cn (M.Y.)

[2] ChinaPetroChina North China Oilfield Branch, Renqiu 062550, China; yjy_syl@petrochina.com.cn (Y.S.); wty_zrr@petrochina.com.cn (R.Z.)

* Correspondence: lujungang21@sohu.com; Tel.: +86-19180967532

Abstract: The well-developed mudstone and gypsum mudstone in the Oligocene Linhe Formation (E_3l) in the Hetao Basin are the main source rocks for gypsum. However, the sedimentary environment and organic matter (OM) enrichment factors of E_3l are not clear, and this inhibits the prediction of hydrocarbon source rock distribution and resource calculation. Major and trace elements, total organic carbon (TOC), pyrolysis using the Rock-Eval II, and saturated hydrocarbon gas chromatography–mass spectrometry (GC–MS) analyses were performed in this study. The results show that E_3l was deposited in brackish water and saline–ultrasaline water, with weak oxidation reduction in an arid and hot environment. Terrestrial input inhibits OM enrichment, while the redox, paleosalinity, paleoclimate, and paleoproductivity play a catalytic role. The main controlling factors of the same lithologic source rocks are different: terrestrial input and paleoclimate have a greater impact on mudstone, and the redox and paleosalinity were more favorable to gypsum mudstone. Although the main controlling factors are different for different lithologies, their OM enrichment characteristics are still consistent. The E_3l water body was deep, and the contribution of nutrients from terrigenous debris to OM enrichment was less. In addition, the water retention environment changed significantly during the E_3l sedimentary period, resulting in fewer nutrients, which limited the improvement of surface water paleoproductivity. The arid climate increased water evaporation and salinity, which to some extent prevented consumption and decomposition. Weak oxidation-reduction fluctuations and the stratification of the water body were obvious, and this was not only conducive to the enrichment of OM but also to its preservation.

Keywords: saline lake; organic enrichment; paleoenvironment; source rock; Hetao Basin

check for updates

Citation: Fu, X.; Lu, J.; Shi, Y.; Zhou, R.; Chen, S.; Yuan, M. Sedimentary Environment and Organic Matter Enrichment Model of Saline Lake Source Rock in the Linhe Depression, Hetao Basin, China. *Processes* **2023**, *11*, 2114. https://doi.org/10.3390/pr11072114

Received: 16 June 2023
Revised: 8 July 2023
Accepted: 12 July 2023
Published: 15 July 2023

1. Introduction

Many large terrestrial oil and gas fields have been developed in saline lake basins [1–4]. The characteristics of the paleo-sedimentary environment and the development model of source rocks in saline lake facies are important scientific issues in petroleum geology, geochemistry, and lacustrine sedimentology. Compared with freshwater lake basins, the biological development characteristics, sedimentary environment, and organic matter (OM) development models of source rocks in saline lake basins are special [5–7]. First, changes in water salinity affect the development of microorganisms and algae [8,9]. Secondly, the special stratification of sedimentary water in the saline lake basin will lead to corresponding changes in the temperature, light transmittance, and redox properties of sedimentary water with depth, which is more conducive to the production and preservation of OM [9,10]. Finally, saltwater lake basins have obtained abundant hydrocarbon production [11,12], confirming good research prospects.

Typical paleo-sedimentary environments and development models of lacustrine source rocks include the large-scale deep-water anoxic lake basin model, the high-salinity enclosed lake basin model, the medium-deep tropical lake basin model, and the oligotrophic lake basin model [13–17]. Based on the sedimentary theory and previous research experience, the study of the paleo-sedimentary environment mainly includes terrestrial input [18], redox conditions [19], paleosalinity [20], paleoclimate [21], paleoproductivity [22], sedimentation rate, paleowater depth [23], etc. Terrestrial inputs introduce plant detritus but also dilute OM availability [18]. Reducing the environment reduces consumption and contributes to OM enrichment [13–19]. Adequate salinity is more conducive to biogenesis [8]. Climate affects water evaporation and is closely related to conservation [24]. Paleoproductivity directly affects the hydrocarbon generation capacity [25]. The sedimentation rate and paleowater depth affect water redox and productivity, and they further affect OM development [23,26].

At present, there are few studies on the source rocks of the Linhe Formation (E_3l) in the Linhe Depression of Hetao Basin. Seismic facies are studied for their source rock distribution [27], organic geochemistry [28], oil source correlation [29], structural prediction of exploration prospects [30], etc. Ancient sedimentary environment characteristics of E_3l mudstone and gypsum mudstone have not been systematically studied. There is no distinction between their sedimentary environments. This is not conducive to the correct assessment of hydrocarbon generation capacity and distribution characteristics. In addition, the ancient sedimentary environment and development model of saline lake source rocks in E_3l are clarified. This can not only enrich the theoretical research of saline lake source rocks but also enrich the content of sedimentology, environmental chemistry, and petroleum geology.

Based on the characteristics of organic geochemistry and the inorganic elements of source rocks, this study will discuss the effects of terrestrial input, redox, paleosalinity, paleoclimate, sedimentation rate, and paleowater depth on organic matter enrichment in mudstone and gypsum-bearing mudstone. It will present an innovative discussion on organic matter enrichment factors in the source rocks of mudstone and gypsum mudstone, and this will also provide a good guiding role in the exploration and development of source rocks in saline lake basins.

2. Geological Setting

The Hetao Basin has an area of approximately 40,000 square kilometers, between the Yinshan and Helan Mountains, and it is adjacent to the Ordos Basin (Figure 1a) [28]. In the regional tectonic position, the basin is sandwiched between the North China plate, the Alxa plate, and the Central Asian orogenic belt [30,31]. The Linhe depression is located in the western part of the basin and has the largest area of 2.43×10^4 km^2, which is the main sedimentary depression and oil-bearing area (Figure 1a,b) [32–34]. It can be divided into the Jilantai sag in the south and the Bayannaoer sag in the north. It has the structural characteristics of east–west zoning and north–south zoning [35]. Among them, the east–west direction of the Bayannaoer sag can be divided into the central fault belt and the Huanghe depression (Figure 1b). The Jilantai sag is divided into the Jixi depression and the Jibei uplift. The basement of the basin is the metamorphic rock series of the Paleoproterozoic–Archaean Wulashan Group. Its stratigraphic distribution is shown in Figure 1c. The Linhe Formation is a better source rock, while the Wuyuan formation is a better cap rock [28].

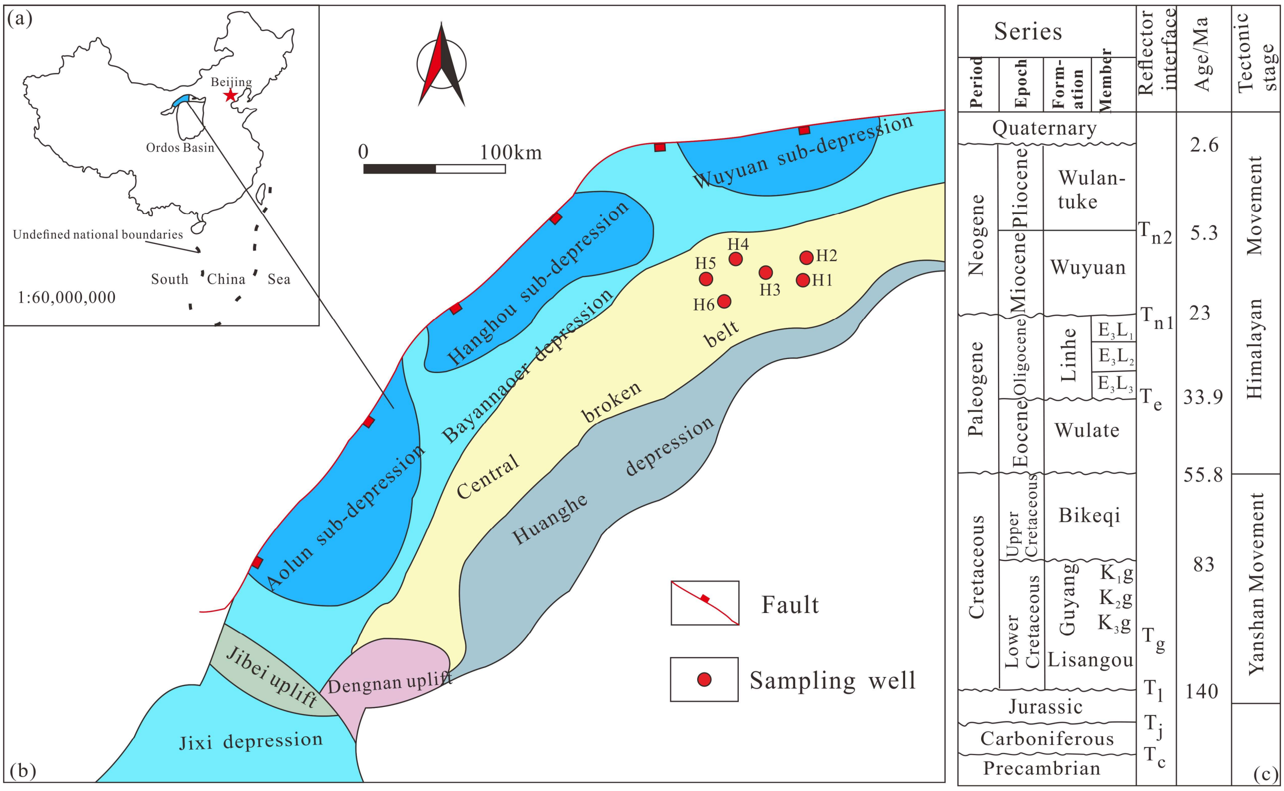

Figure 1. Geographical location map (**a**), tectonic unit division map (**b**), and stratigraphic column map (**c**) of Hetao Basin.

3. Materials and Methods

A total of 78 core samples were collected for experiments. A total of 42 samples (23 mudstones and 19 gypsum mudstones) were used for total organic carbon (TOC), Rock-Eval pyrolysis and saturated hydrocarbon gas chromatography—mass spectrometry (GC–MS). We collected 36 core data (10 mudstones, 11 sandstones, and 15 gypsum mudstones) from the Linhe Formation of well H6 for major and trace element analysis experiments. The sampling location is shown in Figure 1b. The main trace element sampling diagram and core photos are shown in Figure 2. Because the cores shown in both Figure 2a,b are sandstones, this section was not continuously sampled. Lithology of LH-13, LH-14 and LH-15 is a gypsum-bearing argillaceous siltstone, which is summarized as gypsum mudstone in data processing.

Before analysis, the samples were washed and dried with methanol/dichloromethane (1/9) solution and ground to powder. Total organic carbon (TOC) analysis was conducted using a LECO CS-125 carbon sulfur analyzer. Specific analysis steps can be found in Xiao et al. [36]. After the air in the instrument was removed by helium, it was analyzed by a Rock-Eval II instrument and heated to 600 °C. The pyrolysis parameters were recorded according to the analysis steps of Su et al. [37].

GC–MS analysis was performed on Agilent 6890 chromatographic column with Agilent 5975 mass spectrometer detector. The saturated hydrocarbon was separated on a 30 m-long HP-5MS elastic silica capillary column (0.25 mm in diameter and 0.25 μm in wall thickness). The gas chromatography heating program was 50 °C constant temperature for 1 min, then 3 °C/min to 310 °C, and a constant temperature of 30 min. Its carrier gas was at a constant current mode, with a flow rate of 1.0 mL/min.

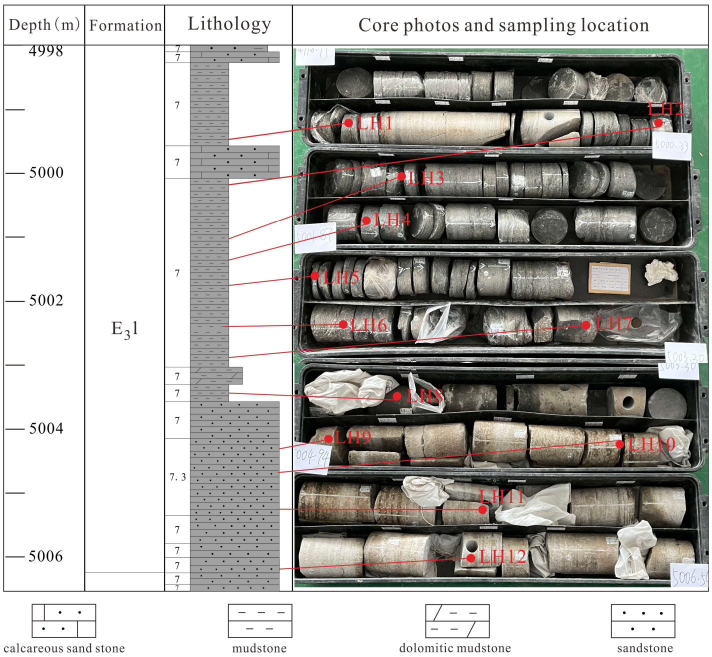

(**a**)

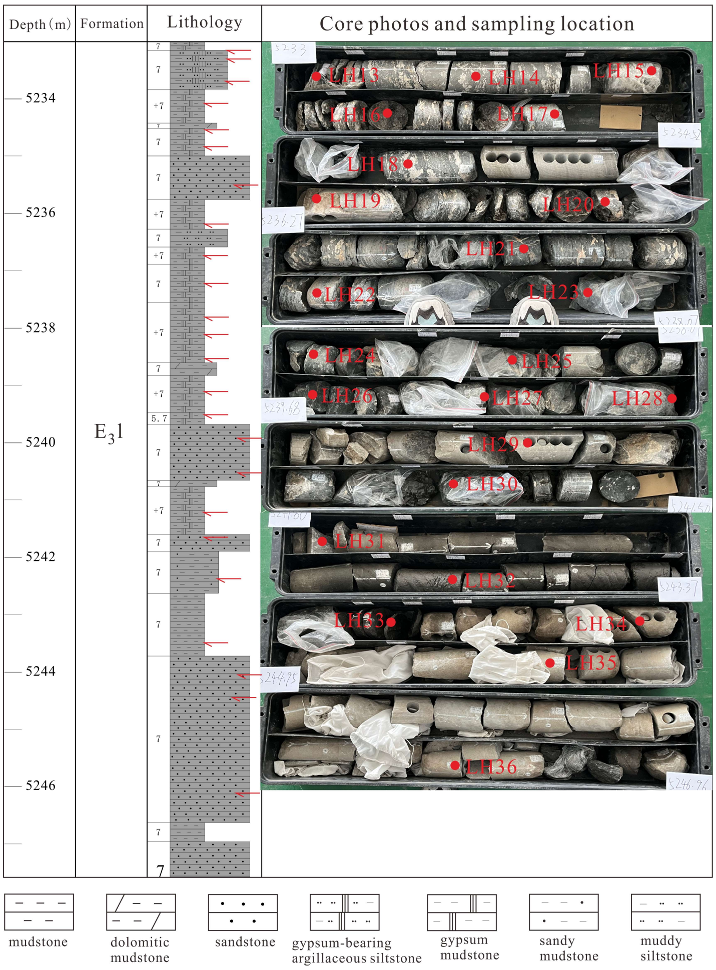

(**b**)

Figure 2. (**a**) Core photos and microelement experimental sampling location map of upper Linhe Formation in well H6. (**b**) Core photos and microelement experimental sampling location map of lower Linhe Formation in well H6.

Major and trace elements have been mentioned many times in the literatures, and the experimental procedures of this current experiment mainly refer to the experimental methods of Wang et al. [38] and Li et al. [27].

Analysis of trace boron was carried out with sodium hydroxide melt on an inductively coupled plasma mass spectrometer (Model 7900). The sample was weighed in a nickel crucible, and the sodium hydroxide flux was added to the sample. After fully mixing, it melted at a high temperature. After cooling, the melt was dissolved and diluted in 100 mL deionized water. An equal amount of HCl was added to the solution, fully mixed, and analyzed by inductively coupled plasma mass spectrometry. After the spectral interference between the elements was corrected, the final analysis result was obtained.

4. Results

4.1. Organic Geochemistry

Table 1 summarizes the geochemical data of source rocks.

Table 1. Statistical table of geochemical data of source rocks in the Linhe Depression, Hetao Basin.

Well	Lithology	Depth (m)	Pr/Ph	Pr/nC$_{17}$	Ph/nC$_{18}$	GI	S$_1$ (mg/g)	S$_2$ (mg/g)	Tmax (°C)	TOC (%)	HI (mg HC/g TOC)
H1	mudstone	3340	0.23	0.31	3.79	1.22	0.31	2.13	424	0.79	269.62
H1	mudstone	3362	0.26	0.13	1.52	0.84	0.75	14.63	416	2.97	492.59
H1	mudstone	3365	0.30	0.45	1.38	1.36	0.75	12.10	418	1.20	1008.33
H1	mudstone	3369	0.14	0.82	6.28	1.27	0.38	10.01	420	1.90	526.84
H1	mudstone	3371	0.19	0.50	3.38	1.35	0.28	1.82	427	0.74	245.95
H1	mudstone	3472	0.34	0.48	1.50	1.82	0.61	1.52	427	0.80	190.00
H1	gypsum mudstone	3450	0.23	0.69	4.63	1.01	0.16	1.05	424	1.52	68.90
H1	gypsum mudstone	3462	0.38	0.49	2.86	0.95	0.09	0.51	416	1.98	25.76
H1	gypsum mudstone	3580	0.20	0.41	4.29	1.10	1.00	0.86	426	0.63	136.51
H1	gypsum mudstone	3710	0.23	0.43	4.18	0.99	0.13	1.26	428	0.64	196.88
H2	mudstone	3635	0.20	0.26	5.19	0.59	0.10	0.97	419	0.51	189.51
H2	mudstone	3758	0.20	0.26	4.80	0.87	0.17	2.66	423	0.81	328.65
H2	mudstone	3855	0.30	0.53	2.78	0.91	0.36	4.25	419	1.18	360.25
H2	gypsum mudstone	3930	0.25	0.43	3.05	0.90	0.17	2.08	429	0.69	301.74
H2	gypsum mudstone	4015	0.27	0.65	3.18	1.14	0.17	1.71	425	0.55	311.67
H2	gypsum mudstone	4130	0.34	0.53	2.38	0.93	0.20	1.98	428	1.58	125.41
H3	mudstone	4197	0.31	0.32	1.96	0.57	0.08	0.26	422	0.11	232.61
H3	mudstone	4215	0.21	0.27	3.50	0.54	0.13	0.92	424	0.44	206.31
H3	mudstone	4236	0.66	0.39	1.68	0.29	0.04	0.11	432	0.22	51.06
H3	mudstone	4238.2	0.87	0.66	1.43	0.60	0.08	1.64	435	0.61	269.38
H3	gypsum mudstone	4238.4	0.52	0.32	0.52	0.28	0.10	0.86	417	0.44	196.99
H3	gypsum mudstone	4238.8	0.42	0.42	1.42	0.16	0.11	0.27	412	0.23	119.39
H3	gypsum mudstone	4242.9	0.26	0.35	0.89	1.07	0.27	0.32	421	0.14	228.43
H3	gypsum mudstone	4243	0.46	0.28	0.56	0.55	0.21	1.20	426	0.49	243.46
H3	gypsum mudstone	4328	0.45	0.35	0.81	0.23	0.53	4.62	424	1.43	323.35
H3	mudstone	4380	0.37	0.50	1.42	0.91	0.73	3.91	421	1.65	236.93
H3	mudstone	4470	0.38	0.66	1.81	0.94	0.27	1.33	418	0.69	191.62
H3	mudstone	4535	0.38	0.54	1.51	1.86	0.19	0.60	417	0.35	172.31
H3	mudstone	4600	0.48	0.73	1.60	1.51	0.15	0.68	418	0.46	147.83
H3	mudstone	4670	0.47	0.66	1.40	1.08	0.17	0.78	419	0.48	162.50
H4	mudstone	4455	0.64	0.42	0.94	0.30	0.08	0.38	422	0.61	61.37
H4	mudstone	4580	0.50	0.50	1.28	0.33	0.11	0.48	421	0.52	91.87
H4	gypsum mudstone	4655	0.42	0.75	2.04	0.57	1.35	13.24	434	3.02	438.30
H4	gypsum mudstone	4750	0.34	0.39	1.11	1.23	1.25	9.20	432	1.29	712.97
H4	gypsum mudstone	4815	0.59	0.84	1.48	0.73	0.09	1.24	434	0.56	222.97

Table 1. *Cont.*

Well	Lithology	Depth (m)	Pr/Ph	Pr/nC_{17}	Ph/nC_{18}	GI	S_1 (mg/g)	S_2 (mg/g)	Tmax (°C)	TOC (%)	HI (mg HC/g TOC)
H5	mudstone	4027	0.31	0.24	2.35	0.71	0.89	18.76	431	2.91	644.54
H5	mudstone	4272	0.32	0.46	2.98	0.63	0.16	2.39	427	0.88	270.77
H5	gypsum mudstone	4397	0.31	0.65	2.38	0.67	0.52	10.29	429	2.08	494.61
H5	gypsum mudstone	4445	0.23	0.64	2.66	0.80	0.14	1.19	425	0.67	178.89
H5	gypsum mudstone	4497	0.41	0.69	1.94	0.90	0.07	0.55	427	0.42	131.81
H5	gypsum mudstone	4553	0.35	0.70	2.00	0.88	0.10	1.26	427	0.64	197.21
H5	mudstone	4650	0.43	0.75	1.82	1.24	0.11	1.00	418	0.53	187.18

TOC represents the total amount of all organic matter in the rock [39,40]. The S_1 represents free hydrocarbon (mg/g), i.e., liquid hydrocarbon content per unit mass of source rock detected at 300 °C. The S_2 (mg/g) represents the amount of kerogen cracked by heating in source rocks from 300 to 600 °C [41,42]. The hydrogen index (HI) is S_2/TOC × 100% [40,41]. The pyrolyzed hydrocarbon (Tmax) maximum temperature represents the temperature corresponding to the highest point of peak S_2, which can be used to indicate OM maturity [43].

The TOC values of mudstone samples in the study area were 0.11–2.97%, with an average of 0.95%. The S_1 value was between 0.04 mg/g and 0.89 mg/g, averaging 0.31 mg/g. The content of S_2 was from 0.11 mg/g to 18.76 mg/g, averaging 3.76 mg/g. The Tmax values were between 416 °C and 435 °C, with an average of 423 °C. The average HI value was 293 mg HC/g TOC. The parameters of gypsum mudstone were similar to mudstone.

Source rock quality can be assessed by TOC and S_2 [40]. The quality of E_3l source rock mudstone and gypsum mudstone in the Hetao Basin was the same, which is distributed from Poor to Very Good (see Figure 3a). OM types are mainly II_2 and III, and some are I and II_1 (Figure 3b). Most source rock samples are distributed between immature and mature (Figure 3b).

In the m/z 85 mass chromatogram of the study area, the peak of pristane (Pr) is lower than that of phytane (Ph). The Pr/Ph ratio of mudstone is 0.14–0.87 (average 0.36), and the parameter of gypsum mudstone is 0.20–0.59 (0.36). In addition, γ and β-carotene are detected in the gypsum mudstone (Figure 4). The source rocks in the study area have high gammacerane. The gammacerane index (gammacerane/C_{30} hopane) (GI) in mudstones is 0.29–1.86 (average 0.97), and the GI ratio in gypsum mudstones is 0.16–1.23 (average 0.77). They all have the 'tail up' phenomenon of C_{31}–C_{35} hopane (Figure 4).

4.2. Geochemistry of Elements

4.2.1. Major Elements

SiO_2 content in the main elements is high, averaging 50.11%, followed by Al_2O_3 and CaO. The Al_2O_3 content is 3.40–18.29%, with an average of 10.89%, and CaO content is 1.25–27.00%, averaging 8.39%. Compared to Union Carbide Corporation (UCC) elements, SiO_2 in sandstone is relatively enriched while other major elements are relatively depleted. The variation trend of elements in mudstone and gypsum mudstone is similar. However, P_2O_5 in mudstone is relatively enriched, and in gypsum mudstone it is relatively depleted (Figure 5, Table 2).

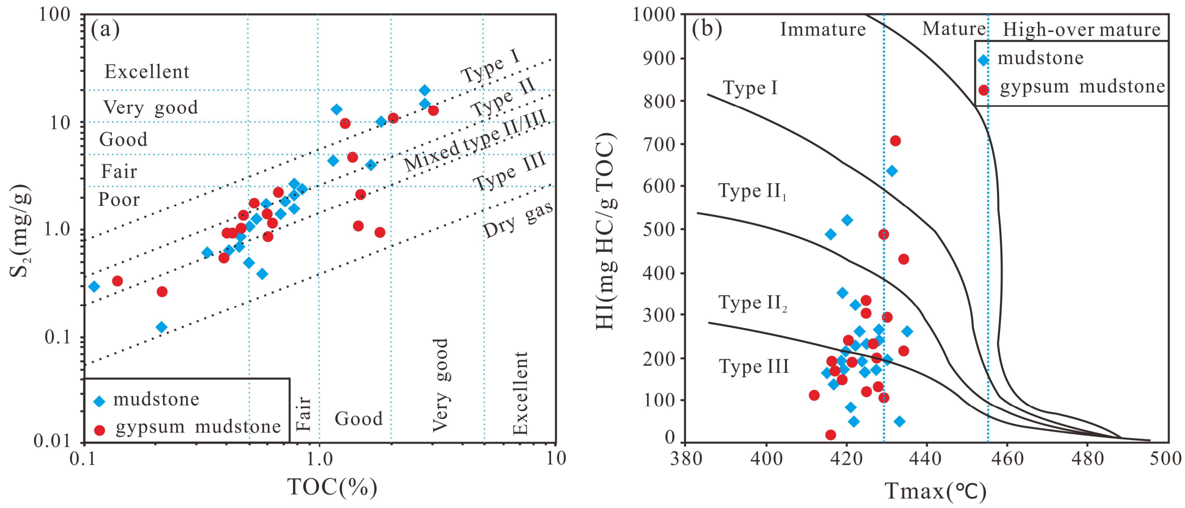

Figure 3. TOC and S_2 cross plot (**a**), the quality classification of source rocks, Tmax and HI cross plot (**b**), and the type classification.

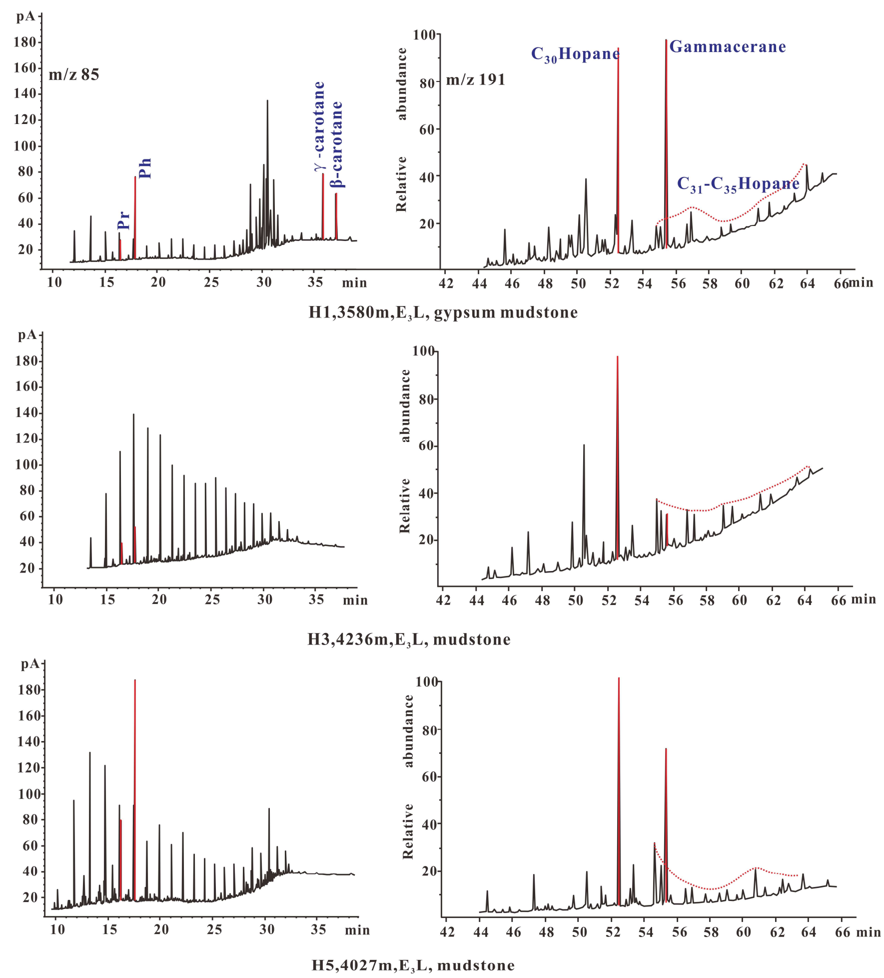

Figure 4. Mass chromatogram of saturated hydrocarbon m/z 85 and m/z 191 of E3l source rocks in the Linhe Depression, Hetao Basin.

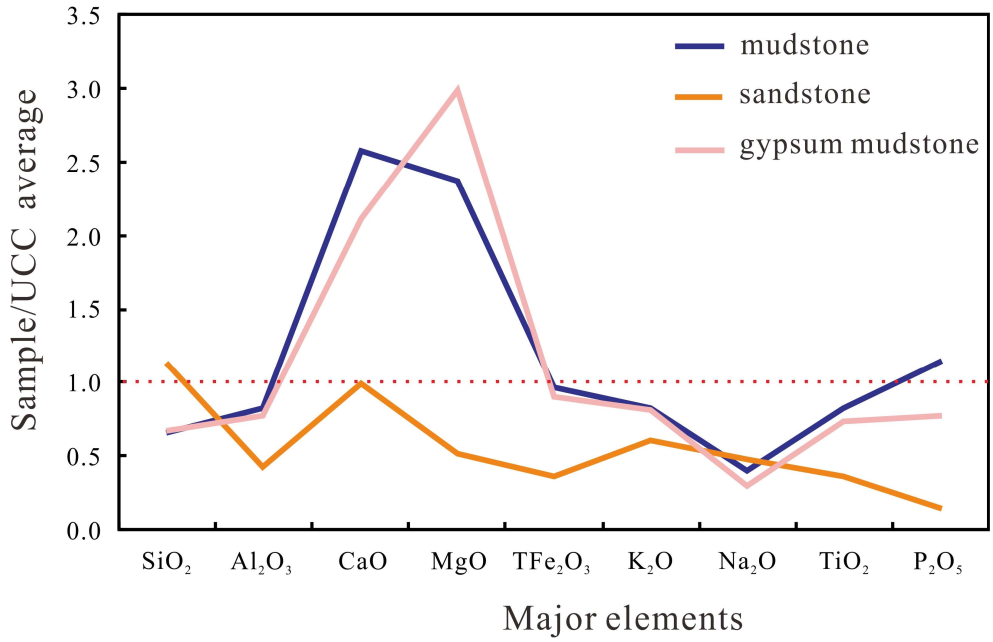

Figure 5. The mean value line chart of major elements/UCC of different lithology in E3l of H6 well.

Table 2. Statistical table of TOC and major elements in the Linhe Formation of well H6.

Number of samples	Depth (m)	Lithology	TOC (%)	SiO_2 (%)	Al_2O_3 (%)	CaO (%)	MgO (%)	TFe_2O_3(%)	K_2O (%)	Na_2O (%)	TiO_2 (%)	P_2O_5 (%)	$Al_2O_3 + K_2O + Na_2O$ (%)
LH-1	4999.8	mudstone	0.219	51.38	15.12	7.26	3.72	5.41	3.45	1.60	0.67	0.35	20.17
LH-2	5000.33	mudstone	0.186	56.23	15.54	5.50	2.84	5.25	3.52	1.66	0.71	0.14	20.72
LH-3	5000.8	mudstone	0.21	53.67	15.10	5.99	2.66	6.21	3.28	1.94	0.68	0.14	20.32
LH-4	5001.13	mudstone	0.17	53.97	16.48	4.89	2.86	6.05	3.67	1.92	0.69	0.14	22.07
LH-5	5001.87	mudstone	0.18	38.47	11.59	10.90	7.96	4.93	2.58	1.62	0.47	0.15	15.79
LH-6	5002.5	mudstone	0.95	33.90	10.32	13.40	9.05	4.47	2.36	1.34	0.40	0.23	14.02
LH-7	5002.9	mudstone	1.81	43.21	12.86	11.60	3.93	5.22	2.82	1.86	0.53	0.14	17.54
LH-8	5003.57	mudstone	0.583	13.33	3.40	27.0	8.81	1.71	0.73	0.65	0.14	0.09	4.78
LH-9	5004.15	sandstone		62.21	4.89	11.00	0.38	1.24	1.66	1.42	0.08	0.01	7.97
LH-10	5004.68	sandstone		77.29	6.77	2.70	0.74	2.04	1.99	2.16	0.23	0.02	10.92
LH-11	5005.35	sandstone		78.69	7.01	2.53	1.23	1.88	1.99	2.25	0.23	0.02	11.25
LH-12	5006.25	sandstone		79.47	6.92	2.10	1.09	2.13	2.07	2.29	0.20	0.02	11.28
LH-13	5233.06	gypsum-bearing argillaceous siltstone	2.36	46.33	13.21	6.37	4.77	5.70	3.07	1.43	0.54	0.17	17.71
LH-14	5233.2	gypsum-bearing argillaceous siltstone	1.86	29.54	8.51	13.65	11.50	3.61	2.00	0.95	0.36	0.11	11.46
LH-15	5233.6	gypsum-bearing argillaceous siltstone	0.213	37.53	8.24	16.35	3.60	3.29	1.78	1.36	0.42	0.10	11.38
LH-16	5234.1	gypsum mudstone	0.166	54.80	18.29	1.25	4.31	6.81	4.76	1.24	0.71	0.12	24.29
LH-17	5234.5	gypsum mudstone	2.01	52.64	16.96	2.45	5.31	6.62	3.88	1.35	0.70	0.18	22.19
LH-18	5234.8	gypsum mudstone	0.151	45.81	14.68	5.74	6.16	6.55	3.49	1.18	0.61	0.16	19.35
LH-19	5235.5	sandstone		61.60	4.78	9.48	4.02	1.52	1.34	1.44	0.11	0.02	7.56
LH-20	5236.17	gypsum mudstone	0.228	17.64	5.66	13.65	19.05	3.29	1.30	0.57	0.22	0.09	7.53
LH-21	5236.73	gypsum mudstone	0.161	49.58	17.14	3.48	5.29	6.92	3.96	1.28	0.67	0.16	22.38
LH-22	5237.2	gypsum mudstone	0.169	34.07	11.35	14.75	4.63	4.29	2.63	0.89	0.48	0.11	14.87

Table 2. *Cont.*

Number of samples	Depth (m)	Lithology	TOC (%)	SiO_2 (%)	Al_2O_3 (%)	CaO (%)	MgO (%)	TFe_2O_3(%)	K_2O (%)	Na_2O (%)	TiO_2 (%)	P_2O_5 (%)	$Al_2O_3 + K_2O + Na_2O$ (%)
LH-23	5237.82	gypsum mudstone	0.0763	46.18	15.04	5.86	7.09	5.89	3.46	1.20	0.59	0.16	19.70
LH-24	5238.1	gypsum mudstone	0.111	46.60	15.97	4.77	6.17	6.41	3.69	1.21	0.64	0.16	20.87
LH-25	5238.55	gypsum mudstone	0.0895	49.01	16.45	4.05	5.88	6.00	3.91	1.16	0.65	0.15	21.52
LH-26	5239.1	gypsum mudstone	0.119	45.54	15.19	6.52	6.17	5.53	3.53	1.11	0.60	0.15	19.83
LH-27	5239.48	gypsum mudstone	0.254	43.06	13.51	9.06	6.39	5.28	3.08	1.10	0.57	0.14	17.69
LH-28	5239.9	sandstone		35.03	10.61	14.15	6.73	4.44	2.39	0.87	0.44	0.12	13.87
LH-29	5240.45	sandstone		65.40	6.52	7.69	2.18	1.55	1.48	1.70	0.25	0.03	9.70
LH-30	5241.19	gypsum mudstone	3.97	23.78	7.38	18.60	11.80	3.07	1.76	0.64	0.30	0.09	9.78
LH-31	5241.6	sandstone		52.43	5.10	13.15	3.16	1.59	1.55	1.16	0.22	0.03	7.81
LH-32	5242.37	sandy mudstone	2.98	63.16	10.03	4.39	4.70	3.43	2.36	1.71	0.46	0.10	14.10
LH-33	5243.5	mudstone	1.47	35.82	11.56	10.80	9.42	4.54	2.89	0.99	0.46	0.10	15.44
LH-34	5244.1	sandstone		77.15	5.18	4.40	0.23	1.67	1.87	1.33	0.41	0.02	8.38
LH-35	5244.5	sandstone		72.28	6.91	4.45	3.16	1.78	2.24	1.68	0.21	0.03	10.83
LH-36	5246.1	sandstone		77.02	7.89	2.19	1.14	2.08	2.56	1.89	0.26	0.03	12.34
		UCC		66.00	15.20	4.20	2.20	5.08	3.40	3.90	0.65	0.15	22.50

4.2.2. Trace Elements

Table 3 summarizes the trace elements content. Enrichment factor (EF) is often used to evaluate the trace elements enrichment [44,45]. The formula is $X_{EF} = (X/Al)_{sample}/(X/Al)_{UCC}$, where X and Al represent element content. The enrichment degree of elements is divided into slight enrichment (EF > 1), moderate enrichment (EF > 3) and strong enrichment (EF > 10), and EF < 1 indicates depleted [44,45]. The calculated trace element enrichment factor profile of the Linhe Formation in the study area is shown in Figure 6. The EF of trace elements obviously changes with lithology and can be divided into four cases, which are represented by four colors in Figure 6.

(1) Ba_{EF}, Na_{EF} and K_{EF} have little difference in mudstone and gypsum mudstone, but they are relatively enriched in sandstone. Na_{EF} is relatively depleted in mudstone and gypsum mudstone (EF < 1), and it is slightly enriched in sandstone (1 < EF < 3). (2) Co_{EF}, Cr_{EF}, Cu_{EF}, Fe_{EF}, Th_{EF}, Ni_{EF} and V_{EF} show the opposite characteristics. They are relatively high in mudstone and gypsum mudstone, and they are depleted in sandstone (EF < 1). (3) P_{EF}, Mn_{EF}, Mo_{EF}, Mg_{EF}, Ca_{EF} and U_{EF} are characterized by moderate enrichment and strong enrichment in lithologic transition areas. (4) Rb_{EF} and Ti_{EF} do not change with lithology. Rb_{EF} is slightly enriched and Ti_{EF} is relatively depleted.

Table 3. Statistical table of trace elements in the Linhe Formation of well H6.

Number of samples	Lithology	Depth (m)	V µg/g	Cr µg/g	Co µg/g	Ni µg/g	Cu µg/g	Sr µg/g	Mo µg/g	Th µg/g	U µg/g	Ba µg/g	Al %	Mg %	Fe %	P µg/g	Rb µg/g	Ca %	Mn µg/g	K %	Na %	Ti %
LH-1	mudstone	4999.8	112	78	16.20	39.20	29.80	222	0.96	13.65	3.50	540	7.53	2.13	3.78	1530	130.50	5.20	899	2.91	1.18	0.37
LH-2	mudstone	5000.33	102	75	17.60	39.50	36.00	184	0.42	13.35	2.30	400	7.54	1.58	3.51	580	125.00	3.85	444	2.88	1.19	0.39
LH-3	mudstone	5000.8	106	76	18.30	42.70	38.90	193	1.23	13.35	2.80	420	7.52	1.50	4.29	610	123.00	4.30	443	2.74	1.39	0.38
LH-4	mudstone	5001.13	114	78	18.40	43.00	42.00	166	0.73	13.35	2.50	400	7.91	1.55	4.04	590	124.50	3.42	386	3.01	1.36	0.37
LH-5	mudstone	5001.87	102	60	15.00	31.00	37.50	349	10.75	9.93	9.20	370	5.74	4.66	3.38	670	99.50	7.72	668	2.17	1.17	0.27
LH-6	mudstone	5002.5	103	57	14.40	33.90	36.40	267	33.40	9.23	11.00	600	5.34	5.50	3.17	1050	95.20	9.53	759	2.06	1.01	0.23
LH-7	mudstone	5002.9	106	65	17.10	40.40	53.70	641	14.15	11.55	12.20	570	6.51	2.27	3.67	600	115.50	8.27	582	2.40	1.39	0.30
LH-8	mudstone	5003.57	30	27	4.60	10.20	10.80	1000	7.27	2.78	6.60	300	1.78	5.29	1.25	410	28.80	19.35	535	0.63	0.53	0.08
LH-9	sandstone	5004.15	8	10	1.40	3.30	4.00	1360	5.16	1.42	0.60	440	2.50	0.22	0.86	40	46.90	8.17	87	1.41	1.07	0.05
LH-10	sandstone	5004.68	18	31	2.60	6.90	6.00	335	1.51	2.48	0.80	660	3.42	0.41	1.50	100	54.30	2.03	213	1.67	1.61	0.13
LH-11	sandstone	5005.35	19	24	2.50	6.30	6.00	229	0.81	2.63	0.90	630	3.52	0.71	1.27	100	53.30	1.90	259	1.67	1.70	0.13
LH-12	sandstone	5006.25	17	24	2.30	6.10	6.20	205	0.73	2.39	0.70	730	3.46	0.63	1.46	70	55.60	1.55	238	1.71	1.68	0.12
LH-13	gypsum-bearing argillaceous siltstone	5233.06	150	73	21.00	46.50	53.80	820	48.80	10.20	22.90	860	6.63	2.76	3.98	690	118.00	4.62	436	2.57	1.06	0.30
LH-14	gypsum-bearing argillaceous siltstone	5233.2	64	41	10.00	24.40	20.00	1345	2.73	7.26	4.10	390	4.34	6.93	2.56	480	76.30	9.71	515	1.71	0.71	0.21
LH-15	gypsum-bearing argillaceous siltstone	5233.6	52	41	8.70	21.30	17.00	1300	3.73	7.56	2.90	290	4.18	2.04	2.28	440	63.10	11.40	426	1.49	1.02	0.23
LH-16	gypsum mudstone	5234.1	118	80	18.60	45.50	36.50	168	1.06	13.65	2.30	360	9.11	2.48	4.66	520	158.50	0.92	282	3.92	0.92	0.39
LH-17	gypsum mudstone	5234.5	121	77	18.10	44.50	36.80	305	1.16	14.45	2.30	460	8.63	3.14	4.65	770	139.00	1.82	471	3.31	1.00	0.39
LH-18	gypsum mudstone	5234.8	116	65	25.00	48.00	37.60	937	11.90	12.80	9.40	520	7.55	3.69	4.58	730	134.00	4.21	540	2.99	0.90	0.35
LH-19	sandstone	5235.5	11	16	1.70	4.30	4.80	1610	0.99	1.60	0.70	840	2.45	2.34	1.01	80	37.00	6.82	341	1.13	1.09	0.07
LH-20	gypsum mudstone	5236.17	61	30	8.10	18.80	18.40	1260	18.60	4.88	10.80	600	2.91	11.45	2.27	360	48.50	9.53	889	1.11	0.42	0.13
LH-21	gypsum mudstone	5236.73	118	70	16.20	41.40	32.70	227	1.03	14.15	2.30	340	8.41	3.01	4.70	700	140.00	2.46	439	3.22	0.92	0.37
LH-22	gypsum mudstone	5237.2	81	52	14.10	30.90	29.70	1030	0.93	9.17	2.20	560	5.64	2.64	2.95	480	92.60	10.20	456	2.18	0.68	0.27
LH-23	gypsum mudstone	5237.82	105	65	15.10	37.50	29.20	201	1.65	12.20	3.30	300	7.48	4.14	4.07	670	124.00	4.19	727	2.88	0.87	0.33
LH-24	gypsum mudstone	5238.1	113	70	21.70	47.90	36.10	299	1.24	14.05	3.30	400	7.99	3.60	4.43	660	135.50	3.42	546	3.07	0.89	0.36
LH-25	gypsum mudstone	5238.55	118	71	16.40	42.50	32.50	240	3.76	13.80	3.90	370	8.25	3.46	4.15	660	140.50	2.92	484	3.20	0.88	0.37
LH-26	gypsum mudstone	5239.1	110	62	15.80	37.30	32.60	374	6.43	12.70	5.10	350	7.57	3.60	3.85	630	128.00	4.66	531	2.94	0.81	0.34
LH-27	gypsum mudstone	5239.48	97	54	12.20	30.90	20.10	904	0.57	11.15	1.70	660	6.85	3.77	3.69	620	114.00	6.55	519	2.61	0.85	0.32
LH-28	sandstone	5239.9	77	43	10.60	26.90	22.20	1060	2.12	9.00	2.40	390	5.31	3.97	3.11	510	83.80	10.00	660	2.01	0.65	0.25
LH-29	sandstone	5240.45	18	17	3.10	6.60	6.60	1395	1.03	3.68	0.80	360	3.17	1.22	1.01	150	43.20	5.41	198	1.19	1.23	0.14
LH-30	gypsum mudstone	5241.19	58	38	9.60	23.30	23.40	1200	8.78	6.71	9.20	350	3.74	7.05	2.03	410	68.40	12.65	542	1.46	0.50	0.17
LH-31	sandstone	5241.6	16	21	2.90	6.50	6.80	5420	0.95	3.33	0.90	100	2.56	1.80	1.03	140	47.60	9.18	325	1.27	0.87	0.12
LH-32	sandy mudstone	5242.37	53	46	9.00	23.70	20.80	1090	1.26	7.99	1.90	800	4.99	2.79	2.27	460	80.50	3.12	372	1.96	1.27	0.26
LH-33	mudstone	5243.5	100	62	17.40	42.20	38.50	356	32.90	9.73	12.20	660	5.81	5.72	3.00	450	112.00	7.57	492	2.40	0.73	0.27
LH-34	sandstone	5244.1	12	18	2.50	4.50	8.10	971	2.78	3.13	2.60	500	2.57	0.13	1.09	70	51.00	3.20	127	1.53	0.99	0.22
LH-35	sandstone	5244.5	18	17	3.00	6.90	8.40	199	1.16	2.98	1.00	680	3.37	1.80	1.16	120	63.00	3.15	305	1.84	1.22	0.12
LH-36	sandstone	5246.1	20	23	3.40	8.40	7.50	443	1.21	3.95	0.80	1120	3.85	0.65	1.42	150	71.00	1.60	203	2.09	1.38	0.15
UCC			107	83	17.00	44.00	25.00	350	1.50	10.70	2.80	550	8.04	1.33	3.50	700	112.00	3.00	600	2.80	2.89	0.41

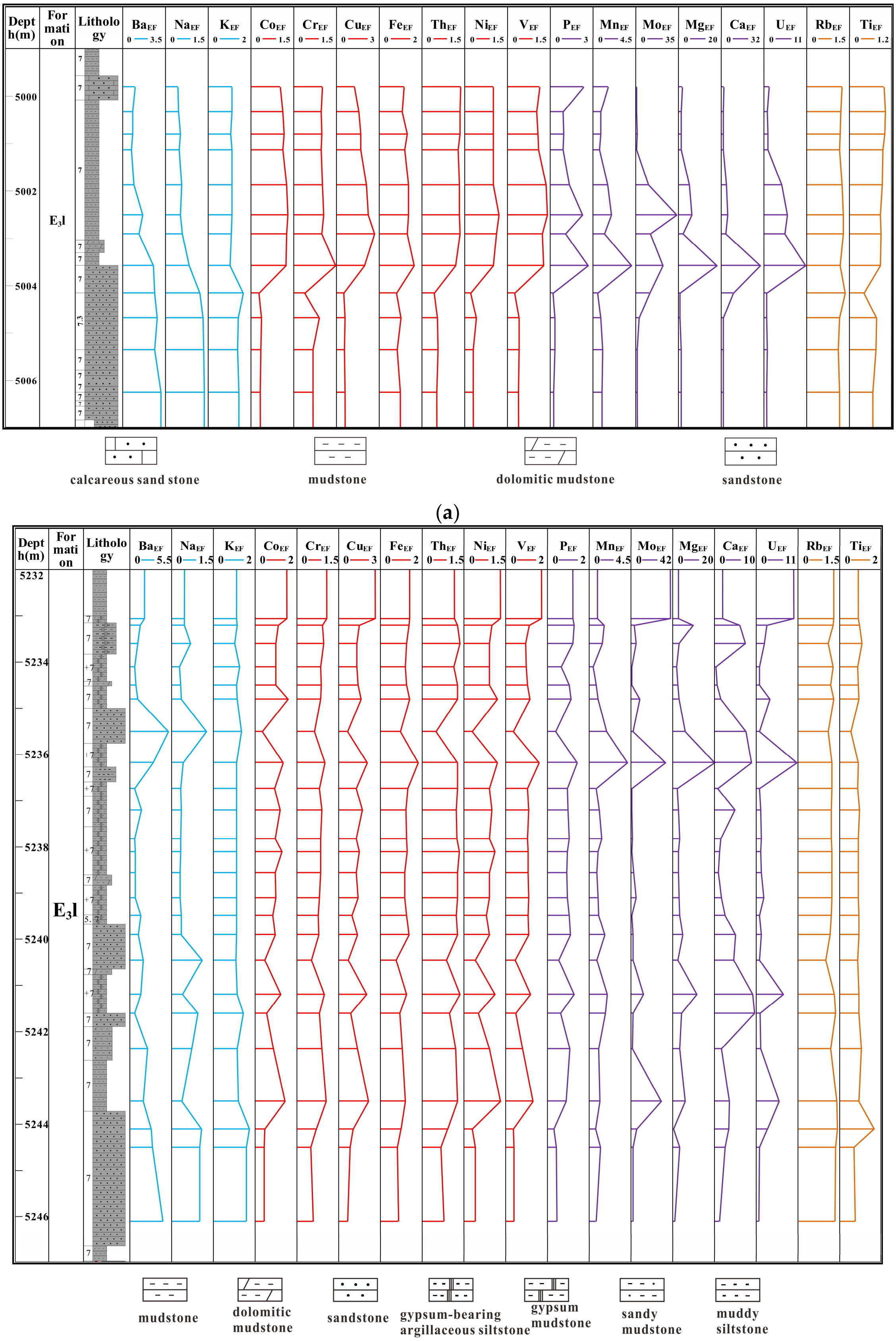

Figure 6. (**a**) Profile of trace element enrichment factor in the upper Linhe Formation of well H6. (**b**) Profile of trace element enrichment factor in the lower Linhe Formation of well H6.

4.2.3. Rare Earth Elements

Rare Earth Elements (REEs) are generally divided into light rare earth elements (LREEs) and heavy rare earth elements (HREEs). LREEs include La~Eu, while HREEs include Gd~Lu [46–48]. Due to the strong stability of REEs, they are often used in paleo-sedimentary environment analysis [48,49]. The average ∑REEs is 134.6 μg/g in mudstone, 47.7 μg/g in sandstone and 149.4 μg/g in gypsum mudstone. The average value of ∑REEs in UCC is 146.4 μg/g, and the gypsum mudstone is higher than the Union Carbide Corporation (UCC), while the mudstone is lower. The differentiation degree of ∑REEs can be reflected by the ratio of LREEs to HREEs ∑LREEs/∑HREEs [50–53]. The average value of ∑LREEs /∑HREEs in mudstone is 10.32, in sandstone 9.63, and in gypsum mudstone 10.65. The ratio of mudstone and gypsum mudstone is similar, which is higher than UCC (average 9.54) (Table 4), indicating that the differentiation is large, the LREEs are enriched and the HREEs are depleted. The mean slope ($(La/Yb)_N$) of the UCC-normalized REE distribution pattern in mudstone is 1.28, and that in gypsum mudstone is 1.33 (Figure 7), indicating weak LREEs. Values less than 1 in Figure 7 are all sandstone samples.

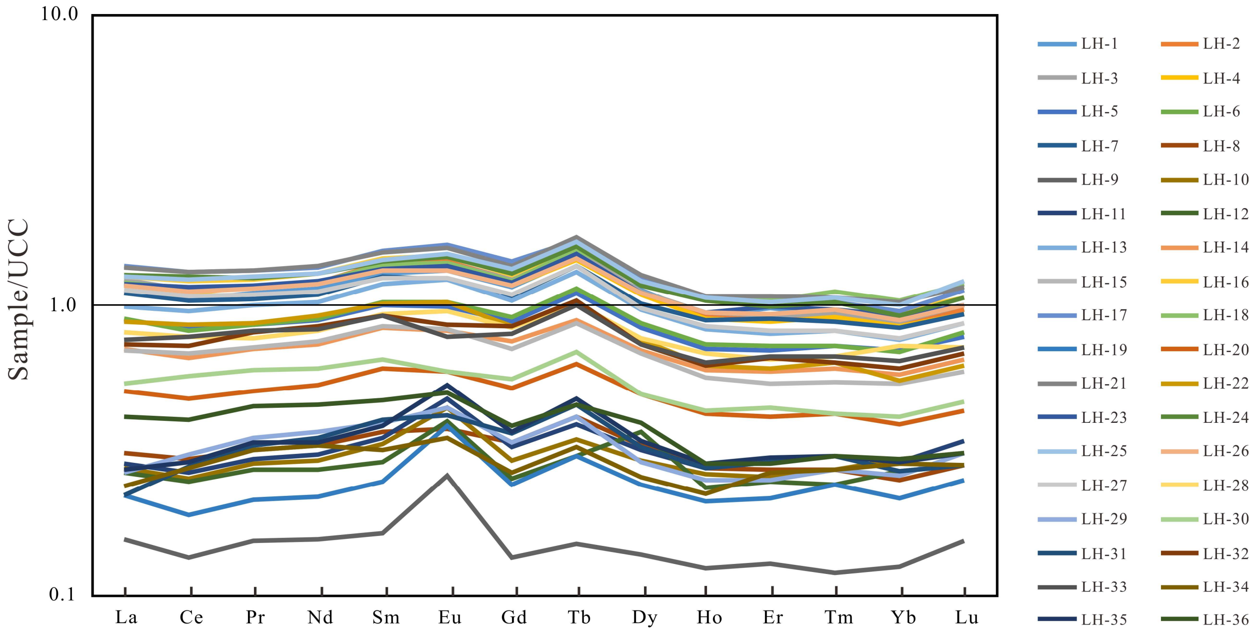

Figure 7. UCC normalized distribution curve of rare earth elements in the Linhe Formation.

Table 4. Statistical table of rare earth elements in the Linhe Formation of well H6.

Number of Samples	Lithology	Depth m	La μg/g	Ce μg/g	Pr μg/g	Nd μg/g	Sm μg/g	Eu μg/g	Gd μg/g	Tb μg/g	Dy μg/g	Ho μg/g	Er μg/g	Tm μg/g	Yb μg/g	Lu μg/g	∑REE	∑LREE	∑HREE	∑ LREE/∑ HREE	$(La/Yb)_N$
LH-1	mudstone	4999.8	33.10	67.10	7.86	29.70	5.83	1.17	4.39	0.67	3.98	0.74	2.25	0.31	1.98	0.32	159.40	144.76	14.64	9.89	1.23
LH-2	mudstone	5000.33	35.70	74.10	8.27	31.20	6.28	1.25	4.67	0.69	3.91	0.75	2.10	0.31	1.90	0.31	171.44	156.80	14.64	10.71	1.38
LH-3	mudstone	5000.8	37.10	72.10	8.32	30.90	6.19	1.24	4.69	0.71	3.93	0.76	2.13	0.31	1.94	0.32	170.64	155.85	14.79	10.54	1.40
LH-4	mudstone	5001.13	33.40	70.30	8.22	31.40	5.98	1.20	4.46	0.66	3.80	0.72	2.03	0.30	1.87	0.30	164.64	150.50	14.14	10.64	1.31
LH-5	mudstone	5001.87	26.60	53.90	6.07	23.20	4.52	0.87	3.34	0.51	2.94	0.57	1.61	0.24	1.54	0.25	126.16	115.16	11.00	10.47	1.27
LH-6	mudstone	5002.5	27.10	52.60	6.11	23.50	4.64	0.90	3.45	0.53	3.05	0.59	1.68	0.24	1.52	0.26	126.17	114.85	11.32	10.15	1.31
LH-7	mudstone	5002.9	33.20	66.70	7.49	28.40	5.64	1.08	4.12	0.63	3.55	0.71	2.07	0.29	1.84	0.30	156.02	142.51	13.51	10.55	1.32
LH-8	mudstone	5003.57	9.30	18.95	2.25	8.60	1.66	0.33	1.28	0.19	1.16	0.22	0.63	0.09	0.55	0.09	45.30	41.09	4.21	9.76	1.24
LH-9	sandstone	5004.15	4.70	8.77	1.10	4.10	0.74	0.23	0.52	0.07	0.49	0.10	0.30	0.04	0.28	0.05	21.49	19.64	1.85	10.62	1.23
LH-10	sandstone	5004.68	8.30	16.35	2.04	7.60	1.50	0.39	1.12	0.16	1.02	0.21	0.59	0.09	0.65	0.10	40.12	36.18	3.94	9.18	0.94
LH-11	sandstone	5005.35	8.60	17.00	2.11	8.00	1.57	0.42	1.24	0.18	1.12	0.22	0.67	0.10	0.64	0.11	41.98	37.70	4.28	8.81	0.99
LH-12	sandstone	5006.25	8.00	15.80	1.94	7.10	1.30	0.35	0.96	0.14	1.28	0.19	0.57	0.08	0.59	0.09	38.39	34.49	3.90	8.84	0.99
LH-13	gypsum-bearing argillaceous siltstone	5233.06	29.70	61.30	7.12	26.70	5.36	1.08	3.97	0.60	3.39	0.66	1.85	0.27	1.68	0.28	143.96	131.26	12.70	10.34	1.30
LH-14	gypsum-bearing argillaceous siltstone	5233.2	21.30	42.50	5.05	19.10	3.79	0.72	2.85	0.41	2.46	0.48	1.36	0.20	1.28	0.21	101.71	92.46	9.25	10.00	1.22
LH-15	gypsum-bearing argillaceous siltstone	5233.6	21.10	43.70	5.11	19.60	3.81	0.73	2.69	0.40	2.40	0.45	1.24	0.18	1.19	0.19	102.79	94.05	8.74	10.76	1.30
LH-16	gypsum mudstone	5234.1	38.00	78.20	8.71	33.40	6.52	1.31	4.86	0.74	4.19	0.83	2.29	0.34	2.11	0.34	181.84	166.14	15.70	10.58	1.32
LH-17	gypsum mudstone	5234.5	40.90	83.40	9.38	35.20	6.95	1.42	5.42	0.77	4.40	0.86	2.38	0.34	2.11	0.36	193.89	177.25	16.64	10.65	1.42
LH-18	gypsum mudstone	5234.8	36.10	73.10	8.24	31.20	6.22	1.23	4.62	0.72	4.24	0.83	2.39	0.37	2.30	0.38	171.94	156.09	15.85	9.85	1.15
LH-19	sandstone	5235.5	6.70	12.15	1.53	5.70	1.12	0.34	0.92	0.14	0.85	0.17	0.50	0.08	0.48	0.08	30.76	27.54	3.22	8.55	1.02
LH-20	gypsum mudstone	5236.17	15.20	30.70	3.60	13.90	2.74	0.52	1.98	0.29	1.74	0.34	0.95	0.14	0.86	0.14	73.10	66.66	6.44	10.35	1.30
LH-21	gypsum mudstone	5236.73	40.60	84.10	9.39	35.60	6.85	1.39	5.23	0.79	4.45	0.86	2.47	0.35	2.26	0.37	194.71	177.93	16.78	10.60	1.32
LH-22	gypsum mudstone	5237.2	26.40	55.00	6.18	24.10	4.59	0.91	3.21	0.47	2.66	0.50	1.40	0.21	1.22	0.20	127.05	117.18	9.87	11.87	1.59
LH-23	gypsum mudstone	5237.82	35.70	74.60	8.35	31.60	6.01	1.21	4.56	0.69	3.88	0.76	2.27	0.32	2.03	0.32	172.30	157.47	14.83	10.62	1.29
LH-24	gypsum mudstone	5238.1	38.30	80.20	8.80	33.40	6.38	1.30	4.93	0.74	4.13	0.83	2.27	0.34	2.04	0.34	184.00	168.38	15.62	10.78	1.38
LH-25	gypsum mudstone	5238.55	37.90	78.70	8.98	33.50	6.49	1.33	5.10	0.76	4.28	0.85	2.36	0.35	2.22	0.39	183.21	166.90	16.31	10.23	1.25
LH-26	gypsum mudstone	5239.1	35.00	71.20	8.11	30.90	5.94	1.16	4.44	0.67	3.88	0.76	2.14	0.32	1.96	0.32	166.80	152.31	14.49	10.51	1.31
LH-27	gypsum mudstone	5239.48	34.00	69.30	7.77	29.20	5.61	1.09	4.17	0.63	3.42	0.68	1.88	0.27	1.70	0.28	160.00	146.97	13.03	11.28	1.47
LH-28	sandstone	5239.9	24.40	50.10	5.46	21.20	4.20	0.84	3.20	0.47	2.71	0.55	1.51	0.22	1.60	0.23	116.69	106.20	10.49	10.12	1.12
LH-29	sandstone	5240.45	8.00	19.60	2.50	9.60	1.78	0.39	1.28	0.19	1.01	0.20	0.58	0.09	0.57	0.10	45.89	41.87	4.02	10.42	1.03
LH-30	gypsum mudstone	5241.19	16.20	36.50	4.27	15.80	2.95	0.52	2.12	0.32	1.73	0.35	1.02	0.14	0.91	0.15	82.98	76.24	6.74	11.31	1.31
LH-31	sandstone	5241.6	6.70	17.95	2.34	9.10	1.83	0.37	1.38	0.21	1.14	0.22	0.67	0.10	0.59	0.09	42.69	38.29	4.40	8.70	0.83
LH-32	sandy mudstone	5242.37	22.10	46.40	5.73	22.00	4.15	0.76	3.23	0.48	2.59	0.50	1.52	0.21	1.34	0.22	111.23	101.14	10.09	10.02	1.21
LH-33	mudstone	5243.5	22.80	49.80	5.84	21.50	4.17	0.69	3.05	0.46	2.58	0.51	1.53	0.22	1.42	0.23	114.80	104.80	10.00	10.48	1.18
LH-34	sandstone	5244.1	7.20	17.60	2.27	8.60	1.44	0.31	1.01	0.15	0.90	0.18	0.61	0.09	0.63	0.09	41.08	37.42	3.66	10.22	0.84
LH-35	sandstone	5244.5	8.20	18.55	2.39	8.80	1.74	0.47	1.40	0.22	1.20	0.23	0.69	0.10	0.64	0.10	44.73	40.15	4.58	8.77	0.94
LH-36	sandstone	5246.1	12.40	25.90	3.21	11.80	2.12	0.44	1.46	0.21	1.39	0.23	0.66	0.10	0.65	0.10	60.67	55.87	4.80	11.64	1.40
UCC			30.00	64.00	7.10	26.00	4.50	0.88	3.80	0.64	3.50	0.80	2.30	0.33	2.20	0.32	146.37	132.48	13.89	9.54	1.40

5. Discussion

Table 5 summarizes the data for all the elements discussed in this section. The distribution of these elements on the profile is shown in Figure 8. Table 6 shows the range of some parameters and the reference information.

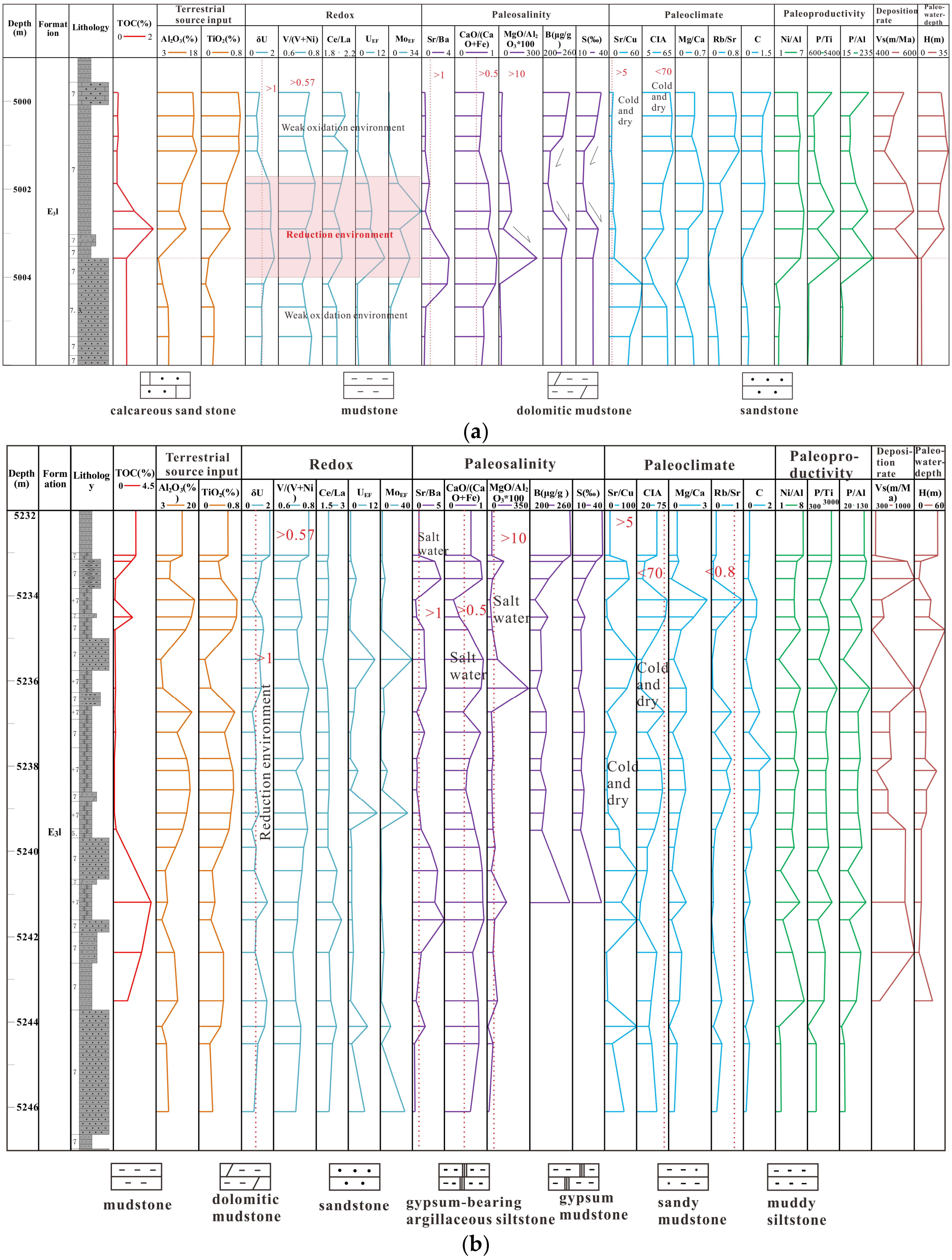

Figure 8. (**a**) Profile of parameter distribution with environmental indication in the upper Linhe Formation of well H6. (**b**) Profile of parameter distribution with environmental indication in the lower Linhe Formation of well H6.

Table 5. Statistical table of parameters indicating environmental significance of inorganic elements in riverfront formation.

Number of Samples	Depth (m)	Lithology	TOC (%)	Terrigenous Input		Redox					Paleosalinity				
				Al_2O_3 (%)	TiO_2 (%)	δU	V/(V+Ni)	Ce/La	U-EF	Mo-EF	Sr/Ba	CaO/(CaO+Fe)	$MgO/Al_2O_3 \times 100$	B(μg/g)	S(‰)
LH-1	4999.8	mudstone	0.22	15.12	0.67	0.87	0.74	2.03	1.33	0.68	0.41	0.66	24.60	248	32.55
LH-2	5000.33	mudstone	0.19	15.54	0.71	0.68	0.72	2.08	0.88	0.30	0.46	0.61	18.28	242	29.43
LH-3	5000.8	mudstone	0.21	15.10	0.68	0.77	0.71	1.94	1.07	0.88	0.46	0.58	17.62	235	26.08
LH-4	5001.13	mudstone	0.17	16.48	0.69	0.72	0.73	2.10	0.91	0.49	0.41	0.55	17.35	213	17.40
LH-5	5001.87	mudstone	0.18	11.59	0.47	1.47	0.77	2.03	4.60	10.04	0.94	0.76	68.68	209	16.09
LH-6	5002.5	mudstone	0.95	10.32	0.40	1.56	0.75	1.94	5.91	33.53	0.45	0.81	87.69	218	19.14
LH-7	5002.9	mudstone	1.81	12.86	0.53	1.52	0.72	2.01	5.38	11.65	1.12	0.76	30.56	243	29.93
LH-8	5003.57	mudstone	0.58	3.40	0.14	1.75	0.75	2.04	10.65	21.89	3.30	0.96	259.12	233	25.18
LH-9	5004.15	sandstone		4.89	0.08	1.12	0.71	1.87	0.69	11.06	3.09	0.93	7.77		
LH-10	5004.68	sandstone		6.77	0.23	0.98	0.72	1.97	0.67	2.37	0.51	0.64	10.93		
LH-11	5005.35	sandstone		7.01	0.23	1.01	0.75	1.98	0.73	1.23	0.36	0.67	17.55		
LH-12	5006.25	sandstone		6.92	0.20	0.94	0.74	1.98	1.30	2.14	0.28	0.59	15.75		
LH-13	5233.06	gypsum-bearing argillaceous siltstone	2.36	13.21	0.54	1.74	0.76	2.06	0.72	1.74	0.95	0.62	36.11	258	38.31
LH-14	5233.2	gypsum-bearing argillaceous siltstone	1.86	8.51	0.36	1.26	0.72	2.00	1.01	1.99	3.45	0.84	135.14	246	31.48
LH-15	5233.6	gypsum-bearing argillaceous siltstone	0.21	8.24	0.42	1.07	0.71	2.07	2.90	5.80	4.48	0.88	43.69	226	22.20
LH-16	5234.1	gypsum mudstone	0.17	18.29	0.71	0.67	0.72	2.06	0.85	1.84	0.47	0.21	23.56	207	15.46
LH-17	5234.5	gypsum mudstone	2.01	16.96	0.70	1.26	0.73	2.04	0.60	1.68	0.66	0.35	31.31	225	21.80
LH-18	5234.8	gypsum mudstone	0.15	14.68	0.61	1.38	0.71	2.02	0.58	1.13	1.80	0.56	41.96	215	18.08
LH-19	5235.5	sandstone		4.78	0.11	1.14	0.72	1.81	9.92	39.45	1.92	0.90	84.10		
LH-20	5236.17	gypsum mudstone	0.23	5.66	0.22	1.23	0.76	2.02	2.71	3.37	2.10	0.86	336.57	217	18.78
LH-21	5236.73	gypsum mudstone	0.16	17.14	0.67	0.66	0.74	2.07	1.99	4.78	0.67	0.43	30.86	210	16.41
LH-22	5237.2	gypsum mudstone	0.17	11.35	0.48	0.84	0.72	2.08	0.72	0.62	1.84	0.83	40.79	223	21.01
LH-23	5237.82	gypsum mudstone	0.08	15.04	0.59	0.90	0.74	2.09	0.77	0.72	0.67	0.59	47.14	224	21.40
LH-24	5238.1	gypsum mudstone	0.11	15.97	0.64	0.83	0.70	2.09	3.58	8.45	0.75	0.52	38.63	216	18.43
LH-25	5238.55	gypsum mudstone	0.09	16.45	0.65	0.92	0.74	2.08	0.82	2.17	0.65	0.49	35.74	215	18.08
LH-26	5239.1	gypsum mudstone	0.12	15.19	0.60	1.09	0.75	2.03	10.66	34.26	1.07	0.63	40.62	223	21.01
LH-27	5239.48	gypsum mudstone	0.25	13.51	0.57	0.63	0.76	2.04	0.79	0.66	1.37	0.71	47.30	220	19.87
LH-28	5239.9	sandstone		10.61	0.44	0.89	0.74	2.05	1.12	0.88	2.72	0.82	63.43		
LH-29	5240.45	sandstone		6.52	0.25	0.79	0.73	2.45	1.27	1.18	3.88	0.88	33.44		
LH-30	5241.19	gypsum mudstone	3.97	7.38	0.30	1.61	0.71	2.25	1.19	0.83	3.43	0.90	159.89	256	37.10
LH-31	5241.6	sandstone		5.10	0.22	0.90	0.71	2.68	1.36	2.44	54.20	0.93	61.96		
LH-32	5242.37	sandy mudstone	2.98	10.03	0.46	0.83	0.69	2.10	1.93	4.55	1.36	0.66	46.86		
LH-33	5243.5	mudstone	1.47	11.56	0.46	1.58	0.70	2.18	0.71	0.45	0.54	0.78	81.49		
LH-34	5244.1	sandstone		5.18	0.41	1.43	0.73	2.44	7.06	12.58	1.94	0.80	4.44		
LH-35	5244.5	sandstone		6.91	0.21	1.00	0.72	2.26	1.09	1.35	0.29	0.79	45.73		
LH-36	5246.1	sandstone		7.89	0.26	0.76	0.70	2.09	6.03	30.35	0.40	0.61	14.45		

Table 5. *Cont.*

Number of Samples	Depth (m)	Lithology	TOC (%)	Paleoclimate					Paleoproductivity			Sedimentation Rate and Paleowater depth	
				Sr/Cu	CIA	Mg/Ca	Rb/Sr	C	Ni/Al	P/Ti	P/Al	Vs	H(m)
LH-1	4999.8	mudstone	0.22	7.45	55.33	0.41	0.59	1.34	5.21	4146.34	203.19	535.57	24.61
LH-2	5000.33	mudstone	0.19	5.11	59.36	0.41	0.68	0.98	5.24	1506.49	76.92	491.38	28.00
LH-3	5000.8	mudstone	0.21	4.96	57.48	0.35	0.64	0.94	5.68	1618.04	81.12	472.47	29.70
LH-4	5001.13	mudstone	0.17	3.94	61.22	0.45	0.75	0.93	5.44	1577.54	74.59	449.18	32.04
LH-5	5001.87	mudstone	0.18	9.31	43.50	0.60	0.29	1.07	5.40	2518.80	116.72	546.24	23.89
LH-6	5002.5	mudstone	0.95	7.34	37.73	0.58	0.36	0.99	6.35	4487.18	196.63	582.03	21.72
LH-7	5002.9	mudstone	1.81	11.94	44.20	0.27	0.18	0.59	6.21	2033.90	92.17	496.37	27.58
LH-8	5003.57	mudstone	0.58	9.26	10.71	0.27	0.00	0.06	5.73	5256.41	230.34	1877.35	3.75
LH-9	5004.15	sandstone		340.00	25.78	0.03	0.03	0.06	1.32	784.31	16.00		
LH-10	5004.68	sandstone		55.83	49.73	0.20	0.16	0.26	2.02	757.58	29.24		
LH-11	5005.35	sandstone		38.17	50.89	0.37	0.23	0.34	1.79	757.58	28.41		
LH-12	5006.25	sandstone		33.06	51.74	0.41	0.27	0.29	1.76	608.70	20.23		
LH-13	5233.06	gypsum-bearing argillaceous siltstone	2.36	15.24	54.98	0.60	0.14	0.36	7.01	2300.00	104.07	363.28	44.05
LH-14	5233.2	gypsum-bearing argillaceous siltstone	1.86	67.25	33.94	0.71	0.06	0.34	5.62	2296.65	110.60	884.38	11.60
LH-15	5233.6	gypsum-bearing argillaceous siltstone	0.21	76.47	29.75	0.18	0.05	0.31	5.10	1938.33	105.26	1088.02	8.50
LH-16	5234.1	gypsum mudstone	0.17	4.60	71.71	2.70	0.94	0.81	4.99	1326.53	57.08	466.45	30.28
LH-17	5234.5	gypsum mudstone	2.01	8.29	68.98	1.73	0.46	0.80	5.16	1984.54	89.22	503.13	27.03
LH-18	5234.8	gypsum mudstone	0.15	24.92	58.62	0.88	0.14	0.47	6.36	2091.69	96.69	306.90	56.73
LH-19	5235.5	sandstone		335.42	28.06	0.34	0.02	0.15	1.76	1230.77	32.65		
LH-20	5236.17	gypsum mudstone	0.23	68.48	26.76	1.20	0.04	0.51	6.46	2769.23	123.71	1033.54	9.18
LH-21	5236.73	gypsum mudstone	0.16	6.94	66.40	1.22	0.62	0.99	4.92	1902.17	83.23	595.79	20.97
LH-22	5237.2	gypsum mudstone	0.17	34.68	38.36	0.26	0.09	0.35	5.48	1804.51	85.11	593.21	21.11
LH-23	5237.82	gypsum mudstone	0.08	6.88	58.95	0.99	0.62	1.66	5.01	2030.30	89.57	617.89	19.86
LH-24	5238.1	gypsum mudstone	0.11	8.28	62.40	1.05	0.45	0.98	5.99	1848.74	82.60	376.93	41.68
LH-25	5238.55	gypsum mudstone	0.09	7.38	64.45	1.18	0.59	1.00	5.15	1803.28	80.00	561.89	22.90
LH-26	5239.1	gypsum mudstone	0.12	11.47	57.75	0.77	0.34	0.89	4.93	1863.91	83.22	570.55	22.38
LH-27	5239.48	gypsum mudstone	0.25	44.98	50.58	0.58	0.13	0.39	4.51	1937.50	90.51	849.00	12.33
LH-28	5239.9	sandstone		47.75	37.91	0.40	0.08	0.51	5.07	2056.45	96.05		
LH-29	5240.45	sandstone		211.36	37.51	0.23	0.03	0.13	2.08	1102.94	47.32		
LH-30	5241.19	gypsum mudstone	3.97	51.28	26.03	1.23	0.06	0.40	6.23	2356.32	109.63	838.65	12.56
LH-31	5241.6	sandstone		797.06	24.34	0.20	0.01	0.06	2.54	1176.47	54.69		
LH-32	5242.37	sandy mudstone	2.98	5.24	54.33	0.89	0.07	0.24	4.75	1755.73	92.18	1059.39	8.85
LH-33	5243.5	mudstone	1.47	9.25	44.11	0.76	0.31	0.61	7.26	1679.10	77.45	429.86	34.22
LH-34	5244.1	sandstone		119.88	40.55	0.04	0.05	0.11	1.75	324.07	27.24		
LH-35	5244.5	sandstone		23.63	45.25	0.57	0.32	0.38	2.05	1043.48	35.61		
LH-36	5246.1	sandstone		59.07	54.34	0.41	0.16	0.15	2.18	1027.40	38.96		

Table 6. Scope of some parameters and references.

Meaning of Indication	Parameter	Content	References		
Terrigenous input	Al_2O_3 TiO_2	The greater the ratio, the greater the terrestrial input	[27,44]		
		Oxidation	Weak oxidation	Reducing	References
Redox	δU	<1		>1	[33]
	V/(V + Ni)	<0.46	0.46–0.57	>0.57	[50]
	Pr/Ph	>3	1–3	<1	[40]
		Fresh water	Brackish water	Salt water	References
Paleosalinity	Sr/Ba	<0.5	0.5–1.0	>1.0	[51]
	CaO/(CaO + Fe)	<0.2	0.2–0.5	>0.5	[52]
	$MgO/Al_2O_3 \times 100$	<1	1~10	>10	[30]
Paleoclimate		Warm and humid	Cold and dry		
	Sr/Cu	1.3~5.0	>5		[53]
	Mg/Ca	High values indicate dry and low values indicate moist			[46]
	Rb/Sr	High values indicate moist, low values indicate dry			
		Cold and dry	Warm and humid	Hot humid	
	CIA	50~70	70~80	80~100	[54]
		Arid climate	Semi-arid to semi-moist climate	Hot humid	
	C	<0.2	0.2~0.8	>0.8	[24]
Paleoproductivity	Ni/Al P/Ti P/Al	The greater the ratio, the greater the ancient productivity	[3,12]		

5.1. Terrigenous Input

Input from terrestrial debris can have multiple effects on OM enrichment [54,55]. As a diluent, it directly reduces OM content, or carries terrigenous OM into the lake bottom, increasing sediment abundance. Preservation of underwater sediments can also be disrupted by affecting burial rates [39,56]. Al and Ti are the main components of the continental crust. Due to the low Ti content in the samples, Al_2O_3 and TiO_2 are used to characterize the terrestrial input (Table 6). Depending on the profile changes, the terrigenous input in mudstone and gypsiferous mudstone is similar, while that in sandstone is significantly lower (Figure 8). By analyzing the correlation between Al_2O_3, TiO_2 and TOC, the Hetao Basin terrestrial input is used as a diluent to reduce the content of OM, which is not conducive to the enrichment (Figure 9a,b). The influence of terrestrial input on mudstone is greater than that of gypsum mudstone.

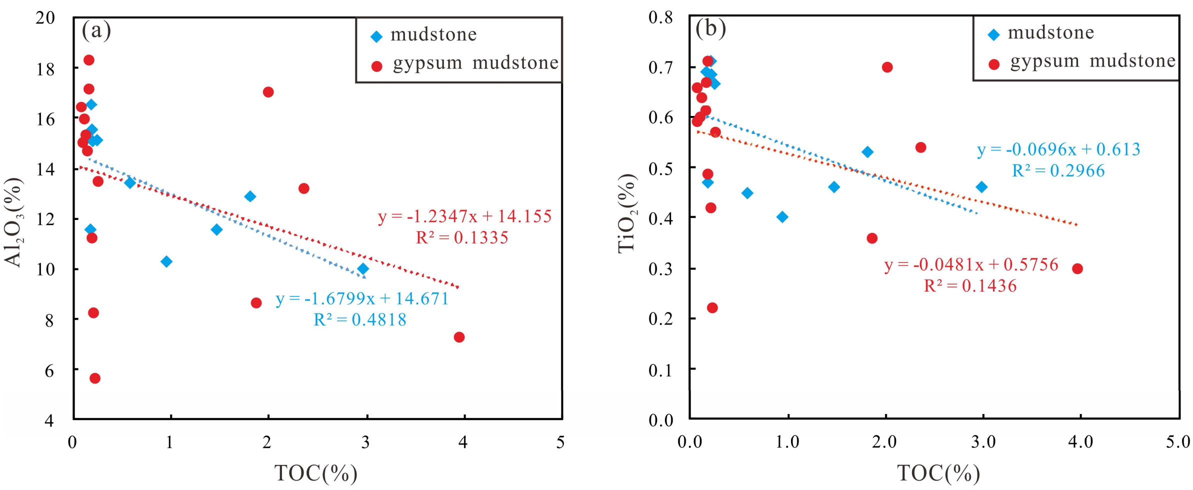

Figure 9. The correlation between elements Al_2O_3 (**a**) and TiO_2 (**b**) and TOC.

5.2. Redox

Biomarker complex parameters Pr/Ph, Gammacerane index (GI) (Gammacerane/C_{30}hopane), Pr/nC_{17} and Ph/nC_{18} may reflect redox and stratification of water bodies [57–59]. The Pr/Ph ratio of less than 1.0 indicates a strong reducing environment [58], and a high GI indicates water stratification and salinity [60]. Through the intersection diagram of Pr/nC_{17} and Ph/nC_{18} parameters (Figure 10a), it is observed that the source rocks in the whole study area are in a strong reducing environment. At the same time, Pr/Ph is less than 1, with a high GI value (Figure 10b), which proves that the E_3l source rocks have strong reduction and water stratification characteristics.

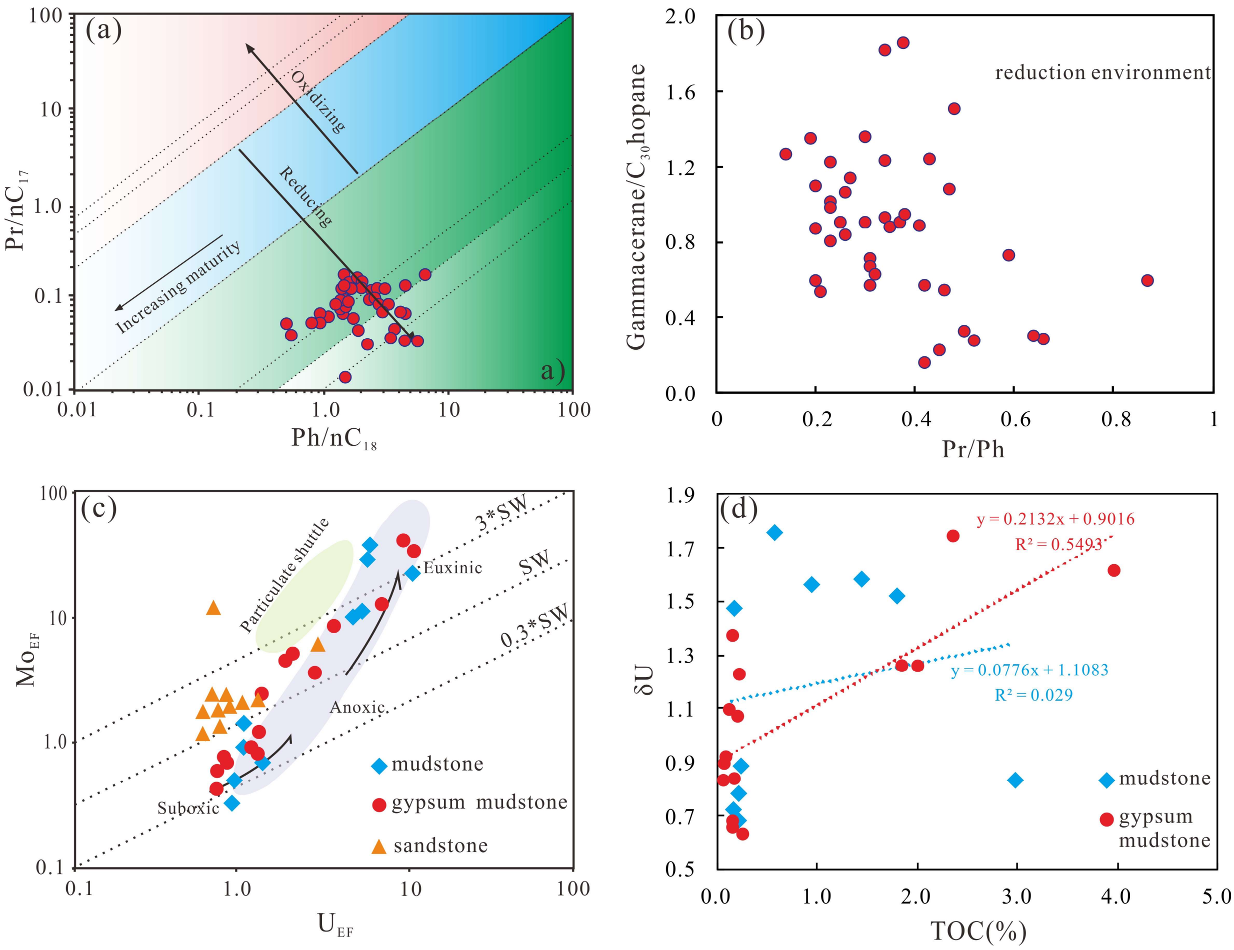

Figure 10. The Pr/nC_{17} and Ph/nC_{18} parameter crossplot (**a**) reflecting the sedimentary environment, and the Pr/Ph and Gammacerane /C_{30}hopane crossplot (**b**). Crossplot of U_{EF} and Mo_{EF} (**c**), and correlation of δU and TOC. SW: modern seawater (**d**).

The concentrations of U and Mo in the continental crust are low (U = 2.8 μg/g, Mo = 1.5 μg/g), which are mainly transported to the ocean through rivers [61]. The concentrations of U and Mo in marine plankton are also low, but the residence time is long. Increased absorption by sediments under anoxic conditions results in better water redox characteristics [61]. Other elements, such as V, Ni, Ce, La and Th, are also sensitive to redox changes. The parameters used in this study were δU (δU = 2 × U/(Th/3 + U), V/(V + Ni) and Ce/La (Table 6) [19].

Based on the results of previous studies, 0.3SW < Mo_{EF}/U_{EF} < SW, SW < Mo_{EF}/U_{EF} < 3SW, 3SW < Mo_{EF}/U_{EF} < 10SW indicate suboxic, anoxic, and euxinic environments (SW is modern seawater), respectively [61]. Source rock samples in the study area are basically located in the purple area in Figure 10c (representing an 'unrestricted ocean' (UM) trend, which is characteristic of the eastern tropical Pacific), and they have an increasing trend with the increase in enrichment coefficient. Other redox parameters showed weak oxidation-reduction changes in the profile (Figure 8), indicating that the water body fluctuated during deposition and that there was obvious stratification. The value of δU in the oxidation parameter changes obviously, and the correlation between this parameter and TOC is selected (Figure 10d). It was found that the source rocks in the study area are enriched with OM with the increase in water reduction, and that gypsum mudstone is more affected than mudstone.

Multiple well data were selected for biomarker parameters, indicating that the Linhe Formation was deposited in a reduced environment. Inorganic elements were analyzed from longitudinal data of a single well. Through comprehensive analysis, the following conclusions can be drawn, the source rocks of E_3l in the Hetao Basin were in a reduced environment as a whole, but the vertical stratification of water bodies was obvious, and there was a weak alternating oxidationreduction transformation phenomenon.

5.3. Paleosalinity

Water salinity is an important indicator of sedimentary environment. This study characterizes paleosalinity from a qualitative and quantitative perspective. The parameters of Sr/Ba, CaO/(CaO + Fe) and $MgO/Al_2O_3 \times 100$, which are sensitive to the change in water salinity, were selected. Their parameter indication ranges are shown in Table 6. The Sr/Ba parameters of the source rocks in the study area are 0.41–4.48 (1.35), and the CaO/(CaO + Fe) ratio is between 0.21 and 0.96, with an average value of 0.66. $MgO/Al_2O_3 \times 100$ is 17.35–336.57 (69.66). According to the changes in the profile in Figure 8, these parameters all have interbedding changes, which reflect that the water body has both brackish water and salt water characteristics during deposition.

Boron (B) is a reliable indicator of salinity in muddy sediments [62,63]. This study measured 23 B elements in mudstone and gypsum mudstone. The formula is established by Li et al., 2003 [64] according to the formula of saline lake basin in China: $LgS = (LgB - 2.0272)/0.2428$. Among them, B is the measured element, S is the ancient salinity (‰), and the use range is 0–40‰. The calculation results are shown in Table 5. Adams (1965) pointed out that the water salinity division standard is S < 10‰ for brackish water–freshwater environment, 10~25‰ for brackish water, 25~35‰ for salty water, and S > 35‰ for ultra-saline water. The paleosalinity of E_3l ranges from 15.46‰ to 38.31‰, with an average value of 23.27‰. There is a change in backwatersaline-ultrasaline water. It shows that there was also stratification of water salinity.

Crossplots of Sr/Ba, CaO/(CaO + Fe), B, and GI parameters characterizing salinity with TOC showed that OM abundance increased with salinity (Figure 11a–c). The correlation between B element and TOC in gypsum mudstone was the best (Figure 11c), indicating that changes in water salinity have the greatest influence on OM enrichment in gypsum mudstone. It is worth noting that TOC increases first and then decreases with the index of GI (Figure 11d). This shows that for the source rocks in the whole study area, TOC increases with the increase in salinity within a certain range, but if salinity is higher, OM abundance may decrease with the increase in salinity. This is consistent with previous conclusions that high salinity is not conducive to biological life [9].

5.4. Paleoclimate

The paleoclimate parameters selected in this study include Sr/Cu, Mg/Ca, Rb/Sr, chemical alteration index (CIA) and C, and their parameter indication ranges are shown in Table 6. $CIA = 100 \times Al_2O_3 \times (Al_2O_3 + NaO + K_2O + CaO^*)$, $CaO^* = CaO - (3 \times P_2O_5/10)$ [54]. $C = \sum(Fe + Mn + Cr + V + Co + Ni)/\sum(Ca + Mg + Sr + Ba + K + Na)$ [24].

Changes in the profile occur through each indicator (Figure 8). The E_3l is in a cold and dry environment as a whole, but the parameters on the profile change, indicating that the climate changes with deposition. Figure 12 shows the correlation between each paleoclimatic index and TOC. Overall, the arid climate is conducive to the enrichment of OM. The TOC correlation between CIA and mudstone and gypsum mudstone is weak

(Figure 12a). Mg/Ca, Rb/Sr and C values have a large influence on the abundance of OM in mudstone, but have little influence on gypsum mudstone (Figure 12b–d).

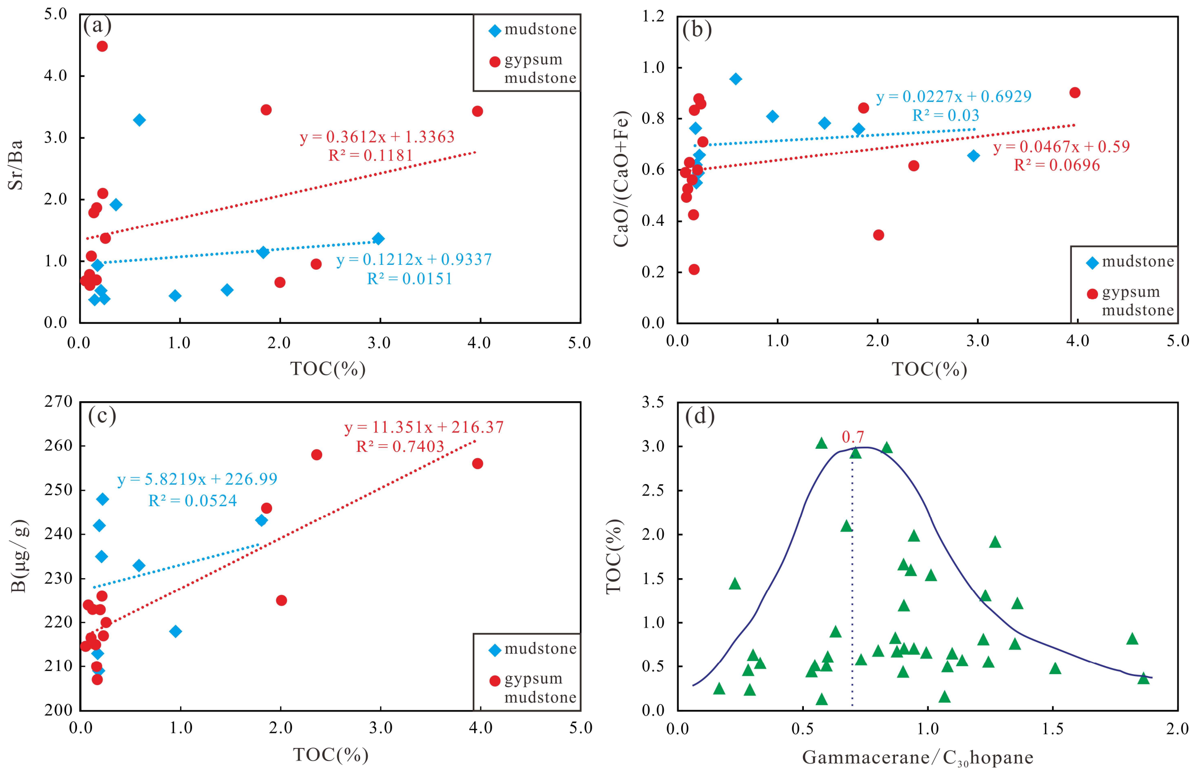

Figure 11. Correlation between paleosalinity parameters and TOC in mudstone and gypsum mudstone. (**a**) Sr/Ba with TOC, (**b**) CaO/(CaO+Fe) with TOC, (**c**) B with TOC, (**d**) Gamma cerane index with TOC.

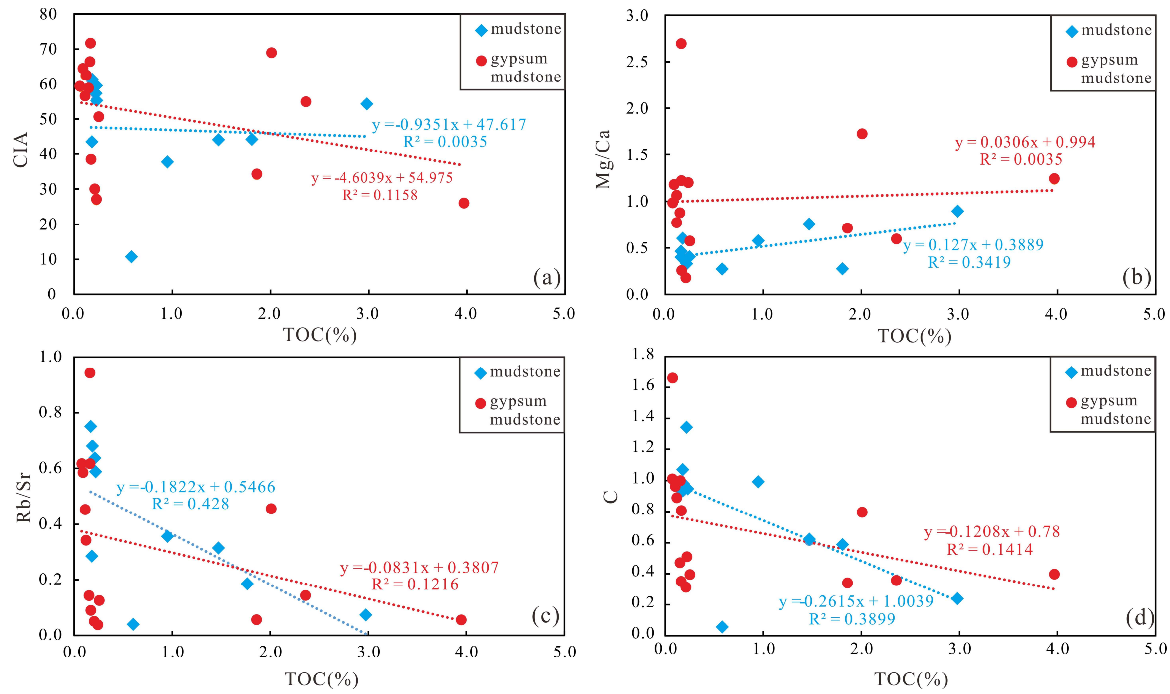

Figure 12. Correlation between paleoclimatic parameters and TOC of mudstone and gypsum mudstone. (**a**) CIA with TOC, (**b**) Mg/Ca with TOC, (**c**) Rb/Sr with TOC, (**d**) C with TOC.

5.5. Paleoproductivity and Water Body Limitation

Paleoproductivity is the basis for the formation of organic-rich sediments [65]. Phosphorus (P) is an important nutrient in the process of biological metabolism. It is also an integral part of the skeleton of many marine organisms and can enter sediments after the organism decomposes [66]. Ni content indicates organic carbon input and also reflects higher paleontological productivity. Ratios of P to Ni and Al to Ti eliminate the effects of P and Ni from land [66]. The increase in paleoproductivity should be conducive to OM enrichment and increased TOC, but the P/Ti and P/Al of mudstone in Figure 13 are inversely proportional to mudstone (Figure 13b,c). The reason may be that the terrestrial input studied in 5.1 has a greater impact on the mudstone, resulting in the ancient productivity shown by the parameters is inversely proportional. If these three abnormal values are ignored, ancient mudstone productivity is positively correlated with TOC.

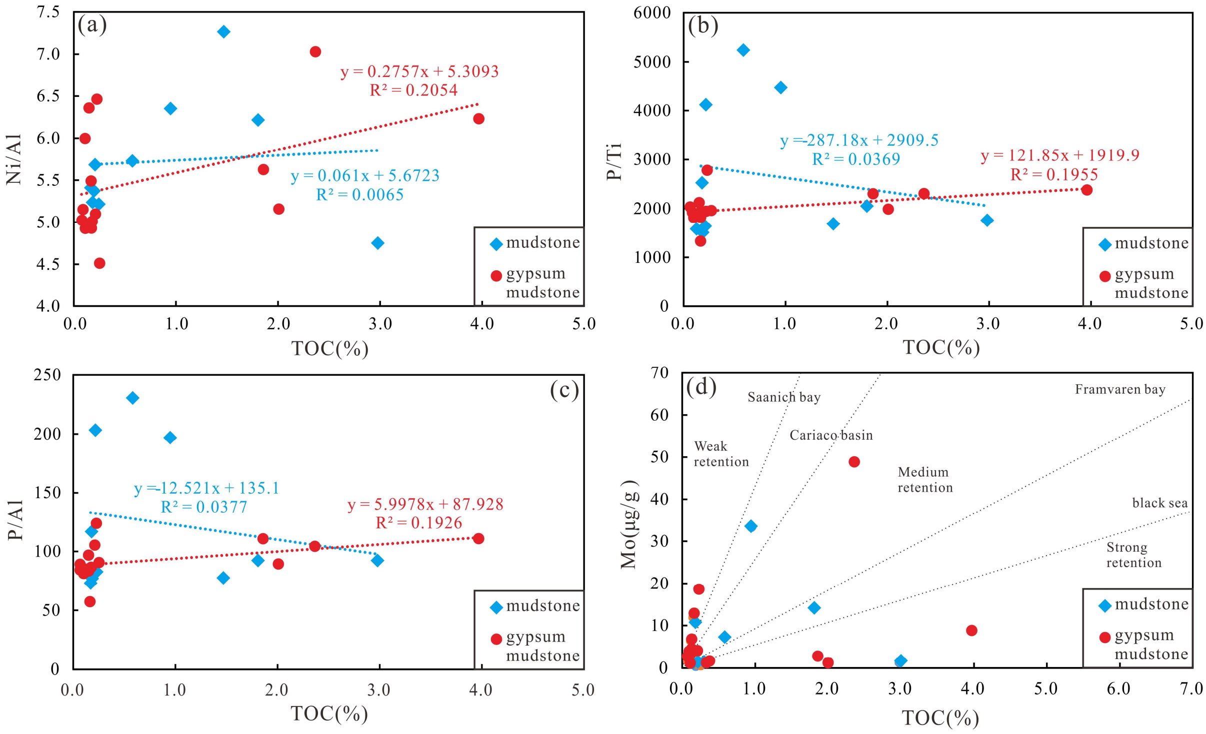

Figure 13. Correlation between Ni/Al (**a**), P/Ti (**b**), P/Al (**c**), Mo (**d**) and TOC in mudstone and p gypsum mudstone.

The connection between basin water and the open sea has an influence on the nutrient supply of surface water in the basin. As the degree of water limitation increases, the exchange between water bodies weakens, and the supply of reducing element Mo from the open sea decreases. According to the restricted degree chart of anoxic water body established by Algeo [66] (Figure 13d), the sample data in the study area are scattered, from weak to strong retention, which is consistent with the conclusion of stratification and fluctuation of the water body.

5.6. Sedimentation Rate and Paleowater Depth

$(La/Yb)_N$ (UCC normalized) is considered to be an effective indicator of REE differentiation. When the value of $(La/Yb)_N$ is close to 1, it indicates that the degree of REE differentiation is weak or there is almost no differentiation, indicating a high deposition rate. If the $(La/Yb)_N$ value is significantly higher or lower than 1, it reflects a low deposition rate [26]. The $(La/Yb)_N$ ratios of the source rocks in the study area are 0.83–1.58, with an average of 1.22, indicating that the E_3l source rocks have a high deposition rate during deposition.

The Co element method is a commonly used quantitative index of paleowater depth. It mainly uses Co element and deposition rate to restore paleowater depth. The calculation formula of the deposition rate with Co is based on Wu and Zhou, 2000 [67]: Vs = Vo × Nco/(Sco-t × Tco). Vs is the deposition rate of the sample; Vo is the deposition rate of normal lakes, 300m/Ma; Nco is the mass fraction of Co in normal lake sediments, 20 ppm; Sco is the abundance of Co in the sample μg/g, and t is the ratio of La abundance in the test sample to the average value of La in the terrigenous clastic rock (31 μg/g). Tco represents the abundance of Co in terrigenous clastic rocks (4.68 μg/g). The calculation formula of ancient water depth is $H = 3.05 \times 10^5/(Vs^{1.5})$ [67]. The calculation results are shown in Table 5. The deposition rate ratio is between 306.90 and 1877.35 μg/g, with an average of 666.58 μg/g, indicating that the E_3l had a high deposition rate. The ancient water depth range is 3.75–56.73 m, with an average of 23.82 m, indicating that the water body was relatively deep.

Sedimentation rate and paleowater depth vary significantly in the profile (Figure 8). However, there is no correlation with TOC change, which has little effect on OM enrichment in the Linhe Formation source rocks.

5.7. Enrichment Model

The environmental control factors of mudstone and gypsum mudstone in E_3l of Hetao Basin are different. Terrestrial input has a stronger inhibitory effect on the enrichment of mudstone OM, and the arid paleoclimate is more favorable. Reducing the environment and salinity of water are more conducive to promoting OM enrichment of gypsum mudstone. For the sampled well H6, the gypsum mudstone deposited earlier than the mudstone, and the main controlling factors of the environment were different in different periods, but for the whole Hetao Basin, the main controlling factors of OM enrichment were unchanged.

There was evidence from the northwest and southeast of the study area [68]. Although the provenance was abundant, the nutrient content was low due to the deep-water body and less input of terrigenous clastic material, which was not conducive to the enrichment of OM in the study area. In addition, the water retention environment changed significantly during the E_3l sedimentary period, resulting in less nutrients, which limited the improvement of surface water paleoproductivity. The above reasons may explain the low TOC in the study area. The arid climate increased water evaporation and salinity, which to some extent prevented the consumption and decomposition of OM. The source rocks in the study area are in a low oxidation-reduction fluctuation environment, and the stratification of the water body is obvious, which is not only conducive to enrichment, but also conducive to preservation (Figure 14).

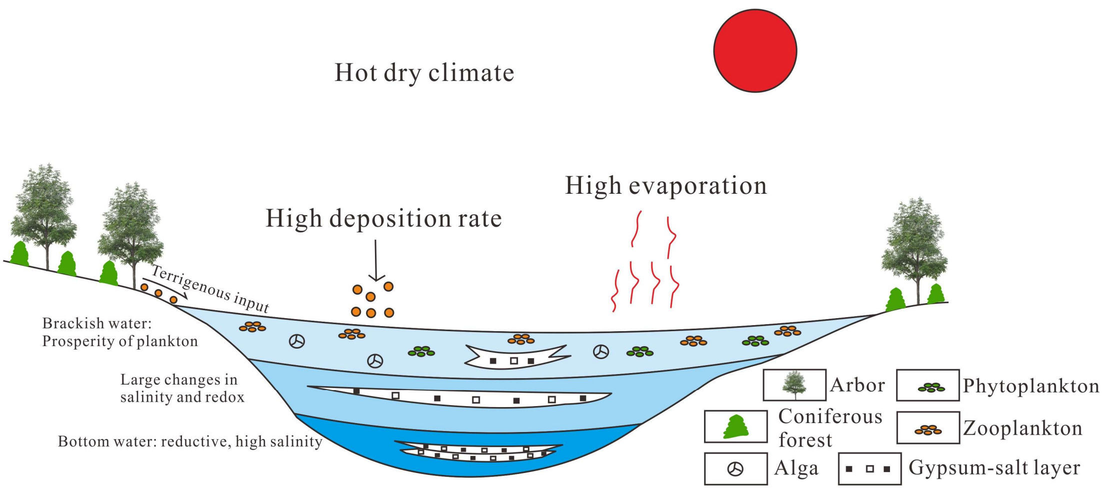

Figure 14. Organic matter enrichment model of E_3l in the Linhe Depression, Hetao Basin.

Both mudstone and gypsum-bearing mudstone can be used as good source rocks, but the environment has different effects on them, which can provide a basis for studying the hydrocarbon generation potential of source rocks. In addition, clarifying the influencing factors of organic matter enrichment can also explain the generally low abundance of organic matter in the saline lake basin.

6. Conclusions

There are two types of source rocks, mudstone and gypsum mudstone, in E_3l of the Hetao Basin, but their hydrocarbon generation potential is the same. By analyzing the characteristics of their sedimentary environment, the following conclusions can be drawn:

1. The correlation between Al_2O_3 and TiO_2 and TOC shows that terrestrial input is used as a diluent to reduce OM content, which is not conducive to enrichment. The effect of terrestrial input on mudstone dilution is greater than that of gypsum mudstone.
2. Pr/Ph, Pr/nC_{17}, Ph/nC_{18}, δU, V/(V + Ni), Ce/La, U_{EF} and Mo_{EF} represent redox. The source rocks of E_3l were in a reduced environment, and there were weak changes in oxidation-reduction in the vertical direction. The more reducing the environment, the more conducive OM enrichment.
3. GI, Sr/Ba, CaO/(CaO + Fe) and MgO/Al_2O_3 $\times$ 100 are used to qualitatively characterize paleosalinity, and B is used for quantitative calculation. Analysis results show that E_3l was in a saline water environment, and there was water stratification on the profile. Paleosalinity promotes OM enrichment, which has a greater impact on gypsum mudstone.
4. The paleoclimatic parameters of Sr/Cu, Mg/Ca, Rb/Sr, CIA and C indicate that the E_3l was in a cold and dry environment, and the arid environment promotes the enrichment of OM, especially for mudstone.
5. Paleoproductivity, water restriction and deposition rate are weakly correlated with TOC, and the water body is deeper.

In this study, good preservation conditions, including reduction conditions, water stratification, and hot and dry climate, were the main controlling factors for OM enrichment. On the basis of clarifying the main controlling factors of organic matter enrichment, further research will be carried out in the future on the hydrocarbon generation mechanism of source rocks and oil and gas resources in the basin.

Author Contributions: X.F.: conceptualization, methodology, writing, and editing. J.L. and S.C.: conceptualization and review. Y.S. and R.Z.: materials provided, project administration. M.Y.: draw and translation. All authors have read and agreed to the published version of the manuscript.

Funding: Funding for this research comes from the "Science and Technology Cooperation Project of the CNPC-SWPU Innovation Alliance" (Nos. 2020CX030000 and 2020CX050000), and "Study on the Control Mechanism of Early Product of Source Rock on Tight Oil Accumulation" (No. 42072185).

Data Availability Statement: All data used to support the findings of this study are included within the article.

Acknowledgments: The authors acknowledge the funding provided, as well as previous research findings related to the study.

Conflicts of Interest: The authors declare that there is no conflict of interest.

References

1. Rabbani, A.R.; Kotarba, M.J.; Baniasad, A.R.; Hosseiny, E.; Wieclaw, D. Geochemical characteristics and genetic types of the crude oils from the Iranian sector of the Persian Gulf. *Org. Geochem.* **2014**, *70*, 29–43. [CrossRef]
2. Mashhadi, Z.S.; Rabbani, A.R. Organic geochemistry of crude oils and Cretaceous source rocks in the Iranian sector of the Persian Gulf: An oil–oil and oil–source rock correlation study. *Int. J. Coal Geol.* **2015**, *146*, 118–144. [CrossRef]
3. Wang, Q.F.; Jiang, F.J.; Ji, H.C.; Jiang, S.; Liu, X.H.; Zhao, Z.; Wu, Y.Q.; Xiong, H.; Li, Y.; Wang, Z. Effects of paleosedimentary environment on organic matter enrichment in a saline lacustrine rift basin–A case study of Paleogene source rock in the Dongpu Depression, Bohai Bay Basin. *J. Pet. Sci. Eng.* **2020**, *195*, 107658. [CrossRef]

4. Hennhoefer, D.; Zell, P.; Stinnesbeck, W. Environmental changes across the Jurassic–Cretaceous boundary in the western proto-Gulf of Mexico—Chemo- and biostratigraphic correlation of NE Mexican sections. *Palaeogeogr. Palaeoclimatol. Palaeoecol.* **2022**, *587*, 110794. [CrossRef]
5. Copetti, D.; Guyennon, N.; Buzzi, F. Generation and dispersion of chemical and biological gradients in a large-deep multi-basin lake (Lake Como, north Italy): The joint effect of external drivers and internal wave motions. *Sci. Total Environ.* **2020**, *749*, 141587. [CrossRef]
6. Liu, Y.; Yao, S.P.; Cao, J.; Xu, C.; Ma, X.X.; Zhang, B.L. Bio-environmental interactions and associated hydrocarbon generation in a saline lake basin: A case study of the Palaeogene interval in the Dongpu Sag, eastern China. *J. Asian Earth Sci.* **2022**, *241*, 105465. [CrossRef]
7. Kifumbi, C.; Schere, C.M.S.; Ros, L.F.D.; Rocha, E.C.D.; Silva, T.F.S.; Angonese, B.S.; Michel, R.D.L. A Pennsylvanian saline-alkaline lake in Gondwana mid-latitude: Evidence from the Piauí Formation chert deposits, Parnaíba Basin, Brazil. *Palaeogeogr. Palaeoclimatol. Palaeoecol.* **2022**, *603*, 111192. [CrossRef]
8. Amils, R.; Ellis-Evans, C. Hinghofer-Szalkay, H. Life in Extreme Environments. *Nature* **2007**, *409*, 1092.
9. Warren, J.K. *Evaporites: A Geological Compendium*; Springer: New York, NY, USA, 2016.
10. He, X.; Lu, J.G.; Li, W.Y.; Zhu, S.B.; Zhao, L.P.; Ma, Z.W.; Zhu, J.; Han, M.M.; Chen, S.J. Geochemical features of source rocks and oil in saline and freshwater lake environments: A case study in the southwest Qaidam Basin. *J. Pet. Sci. Eng.* **2022**, *218*, 110948. [CrossRef]
11. Milleson, M.; Myers, T.S.; Tabor, N.J. Permo-carboniferous paleoclimate of the Congo Basin: Evidence from lithostratigraphy, clay mineralogy, and stable isotope geochemistry. *Palaeogeogr. Palaeoclimatol. Palaeoecol.* **2016**, *441*, 226–240. [CrossRef]
12. Wang, Z.X.; Tang, Y.J.; Wang, Y.L.; Zheng, Y.H.; Chen, F.L.; Wu, S.Q.; Fu, D.L. Kinetics of shale oil generation from kerogen in saline basin and its exploration significance: An example from the Eocene Qianjiang Formation, Jianghan Basin, China. *J. Anal. Appl. Pyrolysis* **2020**, *150*, 104885. [CrossRef]
13. Demaison, G.J.; Moore, G.T. Anoxic environments and oil source bed genesis. *AAPG Bull.* **1980**, *64*, 1179–1209. [CrossRef]
14. Powell, T.G. Petroleum geochemistry and depositional setting of lacustrine source rocks. *Mar. Pet. Geol.* **1986**, *3*, 119–200. [CrossRef]
15. Katz, B.J. Controls on distribution of lacustrine source rocks through time. *AAPG Mem.* **1990**, *50*, 132–139.
16. Adegoke, A.K.; Abdullah, W.H.; Hakimi, M.H.; Sarki Yandoka, B.M. Geochemical characterisation and organic matter enrichment of Upper Cretaceous Gongila shales from Chad (Bornu) Basin, northeastern Nigeria. *Bioprod. Versus Anoxia Cond.* **2015**, *135*, 73–87. [CrossRef]
17. Khaled, A.; Li, R.X.; Xi, S.L.; Zhao, B.S.; Wu, X.L.; Yu, Q.; Zhang, Y.; Li, D.L. Paleoenvironmental conditions and organic matter enrichment of the Late Paleoproterozoic Cuizhuang Formation dark shale in the Yuncheng Basin, North China. *J. Pet. Sci. Eng.* **2021**, *208*, 109627. [CrossRef]
18. Murphy, A.E.; Sageman, B.B.; Hollander, D.J.; Lyons, T.W.; Brett, C.E.E. Black shale deposition and faunal overturn in the Devonian Appa-lachian Basin: Clastic starvation, seasonal water-column mixing, and efficient biolimiting nutrient recycling. *Paleoceanography* **2000**, *15*, 280–291. [CrossRef]
19. Mort, H.; Jacquat, O.; Adatte, T.; Steinmann, P.; Follmi, K.; Matera, V.; Berner, Z.; Stuben, D. The Cenomanian/Turonian anoxic event at the Bonarelli Level in Italy and Spain: Enhanced productivity and/or better preservation? *Cretac. Res.* **2007**, *28*, 597–612. [CrossRef]
20. Compton, J.S. Degree of supersaturation and precipitation of organogenic dolomite. *Geology* **1988**, *16*, 318–321. [CrossRef]
21. Moradi, A.V.; Sari, A.; Akkaya, P. Geochemistry of the Miocene oil shale (Hancili Formation) in the Cankiri-Corum Basin, Central Turkey: Implications for Paleoclimate coditions, source-area wethering, provenance and tectonic setting. *Sediment. Geol.* **2016**, *341*, 289–303. [CrossRef]
22. Longman, J.; Palmer, M.R.; Gernon, T.M.; Manners, H.R. The role of tephra in enhancing organic carbon preservation in marine sediments. *Earth-Sci. Rev.* **2019**, *192*, 480–490. [CrossRef]
23. Kata, B.; Lin, F. Lacustrine basin unconventional resource plays: Key differences. *Mar. Petrol. Geol.* **2014**, *56*, 255–265. [CrossRef]
24. Gradstein, F.M.; Ogg, J.G.; Smith, A.G.; Lourens, L.W.B. New Geological Time Scale, with Special Reference to Precambrian and Neogene. *Episodes* **2004**, *27*, 83–100. [CrossRef]
25. Meng, Q.T.; Liu, Z.J.; Hu, F.; Sun, P.C.; Zhou, R.J.; Zhen, Z. Productivity of Eocene Ancient Lake and Enrichment Mechanism of Organic Matter in Huadian Basin. *J. China Univ. Pet.* **2012**, *36*, 38–44. (In Chinese)
26. Tenger, T.; Liu, W.H.; Xu, Y.C. Comprehensive geochemical identification of highly evolved marine hydrocarbon source rocks: Organic matter, palaeoenvironment and development of effective hydrocarbon source rocks. *Chin. J. Geochem.* **2006**, *25*, 332–339. [CrossRef]
27. Li, C.X.; Liu, Z.; Wang, S.C.; Xu, Z.Y.; Chen, S.G.; You, X.L.; Wang, B. Prediction of major source rocks distribution in the transition from depressed to rifted basin using seismic and geological data: The Guyang to Linhe Formations in the Linhe Depression, Hetao Basin, China. *J. Pet. Sci. Eng.* **2022**, *214*, 110472. [CrossRef]
28. Zhang, R.F.; Lu, J.G.; Shi, Y.L.; Chen, S.G.; Zhou, R.R.; Zhao, R.Q.; Yuan, M.; Zhou, Y.X. Hydrocarbon potential and sedimentary environment of organic matter in source rocks of Linhe and Guyang Formations in Linhe depression, Hetao Basin. *Arab. J. Geosci.* **2022**, *15*, 1866–7511. [CrossRef]

29. Zhao, R.Q.; Chen, S.J.; Fu, X.Y.; He, Z.T. Classification and source of crude oil in the Linhe Depression, Hetao Basin. *Arab. J. Geosci.* **2022**, *15*, 14. [CrossRef]
30. Fu, S.T.; Fu, J.H.; Yu, J.; Yao, J.L.; Zhang, C.L.; Ma, Z.R.; Yang, Y.J.; Zhang, Y. Petroleum geological features and exploration prospect of Linhe Depression in Hetao Basin, China. *Pet. Explor. Dev.* **2018**, *45*, 803–817. [CrossRef]
31. Yin, Y.Y.; Guo, Q.; Li, W.; Liang, P.G. Structural features and favourable areas of the Linhe depression in Hetao Basin, inner Mongolia. *Miner. Explor.* **2020**, *11*, 427–432. (In Chinese)
32. Kong, Q.F.; Li, J.F.M.; Li, M.C.; Wu, K.; Sun, L. Geochemical Characteristics of Gas Source Rock and Generation-Evolution Model of Biogenic Gas in Hetao Basin. *Nat. Gas Geosci.* **2008**, *19*, 238–243. (In Chinese with English abstract)
33. Zhang, R.F.; He, H.Q.; Chen, S.G.; Li, G.X.; Liu, X.H.; Guo, X.J.; Wang, S.C.; Fan, T.Z.; Wang, H.L.; Liu, J.; et al. New understandings of petroleum geology and great discovery in the Linhe depression, Hetao Basin. *China Pet. Explor.* **2020**, *25*, 1–12, (In Chinese with English abstract).
34. Du, X.Y.; Ding, W.L.; Jiao, B.C.; Zhou, Z.C.; Xue, M.W.; Liu, T.S. Characteristics of hydrocarbon migration and accumulation in the Linhe-Jilantai area, Hetao Basin, China. *Pet. Sci. Technol.* **2019**, *37*, 2182–2189. [CrossRef]
35. Ran, Y.K.; Zhang, P.Z.; Chen, L.C. Late Quaternary history of paleoseismicactivity along the Hohhot segment ofthe Daqingshan piedmont fault in Hetao depression zone. *North China Ann. DI Geofis.* **2003**, *46*, 1053–1069. [CrossRef]
36. Xiao, Z.L.; Chen, S.J.; Liu, C.W.; Lu, Z.X.; Zhu, J.; Han, M.M. Lake basin evolution from early to Middle Permian and origin of Triassic Baikouquan oil in the western margin of Mahu Sag, Junggar Basin, China: Evidence from geochemistry. *J. Pet. Sci. Eng.* **2021**, *203*, 108612. [CrossRef]
37. Su, K.M.; Chen, S.J.; Hou, Y.T.; Zhang, H.F.; Zhang, W.X.; Liu, G.L.; Hu, C.; Han, M.M. Geochemical characteristics, origin of the Chang 8 oil and natural gas in the southwestern Ordos Basin, China. *J. Pet. Sci. Eng.* **2021**, *200*, 108406. [CrossRef]
38. Wang, Z.W.; Shen, L.J.; Wang, J.; Fu, X.G.; Xiao, Y.; Song, C.Y.; Zhan, W.Z. Organic matter enrichment of the Late Triassic Bagong Formation (Qiangtang Basin, Tibet) driven by paleoenvironment: Insights from elemental geochemistry and mineralogy. *J. Asian Earth Sci.* **2022**, *236*, 105329. [CrossRef]
39. Sageman, B.B.; Murphy, A.E.; Werne, J.P.; Ver, C.A.; Straeten, D.J.; Hollander, T.W. Lyons A tale of shales: The relative roles of production, decomposition, and dilution in the accumulation of organic-rich strata, Middle–Upper Devonian, Appalachian basin. *Chem. Geol.* **2003**, *195*, 229–273. [CrossRef]
40. Peters, K.; Cassa, M. Applied source rock geochemistry. In *AAPG Memoir 60, the Petroleum System—From Source to Trap*; Magoon, L., Dow, W., Eds.; AAPG: Tulsa, OK, USA, 1994; pp. 93–120.
41. Singh, A.K.; Chakraborty, P.P. Geochemistry and hydrocarbon source rock potential of shales from the Palaeo-Mesoproterozoic Vindhyan Supergroup, central India. *Energy Geosci.* **2021**, *4*, 100073. [CrossRef]
42. Ehsan, D. Geochemistry and origins of Sarvak oils in Abadan plain: Oil-oil correlation and migration studies. *Energy Sources Part A Recovery Util. Environ. Eff.* **2019**, *43*, 716–726. [CrossRef]
43. Tissot, B.P.; Welte, D.G. *Petroleum Formation and Occurrence*, 2nd ed.; Springer: Berlin, Germany, 1984; p. 699.
44. Tribovillard, N.; Algeo, T.W.; Lyons, T.; Riboulleau, A. Trace metals as paleoredox and paleoproductivity proxies: An update. *Chem. Geol.* **2006**, *232*, 12–32. [CrossRef]
45. Algeo, T.J.; Tribovillard, N. Environmental analysis of paleoceanographic systems based on molybdenum–uranium covariation. *Chem. Geol.* **2009**, *268*, 211–225. [CrossRef]
46. McLennan, S.M. Relationship between the trace element composition of sedimentary rocks and upper continental crust. *G-cubed* **2001**, *2*, 203–236. [CrossRef]
47. Pourmand, A.; Dauphas, N.; Ireland, T.J. A novel extraction chromatography and MC-ICP-MS technique for rapid analysis of REE, Sc and Y: Revising CI-chondrite and Post-Archean Australian Shale (PAAS) abundances. *Chem. Geol.* **2012**, *291*, 38–54. [CrossRef]
48. Zeng, J.H.; Lan, X.D.; Liu, H.; Wei, Y.S. Genesis and mechanisms of organic matter enrichment of the Hongshuizhuang Formation in the Zhoukoudian area of Jingxi sag, North China. *J. Palaeogeogr.* **2022**, *11*, 653–677. [CrossRef]
49. Cheng, D.W.; Zhou, C.M.; Zhang, Z.J.; Yuan, X.J.; Liu, Y.H.; Chen, X.Y. Paleo-Environment Reconstruction of the Middle Permian Lucaogou Formation, Southeastern Junggar Basin, NW China: Implications for the Mechanism of Organic Matter. *J. Earth Sci.* **2022**, *33*, 963–976. [CrossRef]
50. Hatch, J.R.; Leventhal, J.S. Relationship between inferred redox potential of the depositional environment and geochemistry of the Upper Pennsylvanian (Missourian) Stark Shale Member of the Dennis Limestone, Wabaunsee County, Kansas, USA. *Chem. Geol.* **1992**, *99*, 65–82. [CrossRef]
51. Bom, M.H.H.; Ceolin, D.; Kochhann, K.G.D.; Krahl, G.; Fauth, G.; Bergue, C.T.; Savian, J.F.; Strohschoen Junior, O.; Simões, M.G.; Assine, M.L. Paleoenvironmental evolution of the Aptian Romualdo Formation, Araripe Basin, Northeastern Brazil. Global Planet. *Change* **2021**, *203*, 103528. [CrossRef]
52. Mukhopadhyay, P.K.; Goodarzi, F.; Crandlemire, A.L. Comparison of coal composition and elemental distribution in selected seams of the Sydney and Stellarton Basins, Nova Scotia, Eastern Canada. *Int. J. Coal Geol.* **1998**, *37*, 113–141. [CrossRef]
53. Lerman, A. *Lakes: Chemistry, Geology, Physics*; Springer: New York, NY, USA, 1978; p. 363.
54. Nesbitt, H.; Young, G.M. Early Proterozoic climates and plate motions inferred from major element chemistry of lutites. *Nature* **1982**, *299*, 715–717. [CrossRef]

55. Harris, N.B.; McMillan, J.M.; Knapp, L.J.; Mastalerz, M. Organic matter accumulation in the Upper Devonian Duvernay Formation, Western Canada Sedimentary Basin, from sequence stratigraphic analysis and geochemical proxies. *Sediment. Geol.* **2018**, *376*, 185–203. [CrossRef]
56. Froelich, P.N.; Klinkhammer, G.; Bender, M.L. Early oxidation of organic matter in pelagic sediments of the eastern equatorial Atlantic: Suboxic diagenesis. *Geochim. Cosmochim. Acta* **1979**, *43*, 1075–1090. [CrossRef]
57. Shanmugam, G. Significance of coniferous rain forests and related organic matter in generating commercial quantities of oil, Gippsland Basin, Australia. *AAPG Bull.* **1985**, *69*, 1241–1254. [CrossRef]
58. Ten Haven, H.L.; de Leeuw, J.W.; Rullkötter, J.; Sinninghe Damsté, J.S. Restricted utility of the pristane/phytane ration as a palaeoenvironmental indicator. *Nature* **1987**, *330*, 641–643. [CrossRef]
59. Summons, R.E.; Hope, J.M.; Swart, R.; Walter, M.R. Origin of Nama basin bitumen seeps: Petroleum derived from a Permian lacustrine source rock traversing southwestern Gondwana. *Org. Geochem.* **2008**, *39*, 589–607. [CrossRef]
60. Sinninghe Damsté, J.S.; Kenig, F.; Koopmans, M.P.; Köster, J.; Schouten, S.; Hayes, J.M.; de Leeuw, J.W. Evidence for gammacerane as an indicator of water column stratification. *Geochim. Cosmochim. Acta* **1995**, *59*, 1895–1900. [CrossRef]
61. Tribovillard, N.; Algeo, T.J.; Baudin, F.; Ribouleau, A. Analysis of marine environmental conditions based onmolybdenum–uranium covariation—Applications to Mesozoic paleoceanography. *Chem. Geol.* **2012**, *324–325*, 46–58. [CrossRef]
62. Walker, C.T.; Price, N.B. Departure Curves for Computing Paleosalinity Boron in lilies and Shales. *AAPG Bull.* **1963**, *47*, 833–841. [CrossRef]
63. Wei, W.; Algeo, T.J. Elemental Proxies for Paleosalinity Analysis of Ancient Shales and Mudrocks. *Geochim. Cosmochim. Acta* **2020**, *287*, 341–366. [CrossRef]
64. Li, J.L.; Chen, D.J. A review of quantitative research methods of paleosalinity. *Pet. Geol. Recovery Effic.* **2003**, *5*, 1–3. (In Chinese)
65. Dymond, J.; Suess, E.; Lyle, M. We used sediment traps to define the higher barium contents in the intermediate and combined our particle flux data with existing water linkages to ocean productivity and the degree of Paleoceanography. *Palaeogeogr. Palaeoclimatol. Palaeoecol.* **1992**, *7*, 163–181. [CrossRef]
66. Algeo, T.J.; Ingall, E. Sedimentary Corg: P ratios, paleocean ventilation, and phanerozoic atmospheric pO2. *Palaeogeogr. Palaeoclimatol. Palaeoecol.* **2007**, *256*, 130–155. [CrossRef]
67. Wu, Z.P.; Zhou, Y.Q. Using the characteristic elements from meteoritic must in strata to calculate sedimentation rate. *Acta Sedimentol. Sin.* **2000**, *8*, 395–399. (In Chinese)
68. Li, C.; Chen, S.J.; Liao, J.B.; Hou, Y.T.; Yu, J.; Liu, G.L.; Xu, K.; Wu, X.T. Geochemical characteristics of the Chang 7 Member in the southwestern Ordos Basin, China: The influence of sedimentary environment on the organic matter enrichment. *Palaeoworld* **2022**, *32*, 429–441. [CrossRef]